

https://dspace.org/

Manganese-Rich Nickel-Manganese-Cobalt Oxides as Hybrid Supercapacitor Electrode Materials

Tshivhase, Funanani

2023-09

University of the Witwatersrand, Johannesburg

https://hdl.handle.net/10539/42146

Tshivhase, Funanani. (2023). Manganese-Rich Nickel-Manganese-Cobalt Oxides as Hybrid Supercapacitor Electrode Materials. [Master's thesis, University of the Witwatersrand, Johannesburg]. https://hdl.handle.net/10539/42146

Downloaded from a DSpace repository. https://dspace.org/

Manganese-Rich Nickel-Manganese-Cobalt Oxides as Hybrid Supercapacitor Electrode Materials



UNIVERSITY OF THE
WITWATERSRAND,
JOHANNESBURG

A dissertation submitted to the Faculty of Science, School of Chemistry, University of the Witwatersrand, for the degree of Master of Science.

Funanani Tshivhase (1725389)

Supervised by:

Prof. Kenneth Ikechukwu Ozoemena

Declaration

I, Funanani Tshivhase, declare this dissertation is my own unaided work, except where stated. It is being submitted for the degree of Master of Science in the Faculty of Sciences, University of the Witwatersrand, Johannesburg. The work contained in this dissertation has not been submitted for any degree or examination in this university or any other university.

Funanani Tshivhase, on this ___20___ day of ___September_____ 2023



Funanani Tshivhase

Dedication

I dedicate this work to my mother, sister, and brothers. They are the reason I never saw giving up as an option in my life. The things I do, the journey I walk, no matter how hard it gets, their love keeps me going. I love them more than life, especially mom.

Acknowledgements

This work wouldn’t have been possible without the supervision of Prof. Kenneth Ikechukwu Ozoemena, who mentored and guided me throughout the journey. He provided emotional and academic support since the beginning of his supervision, which began when I decided to join his research group on my honour studies.

I would also like to acknowledge Dr Aderemi Haruna and Dr Thapelo Mofokeng for always assisting me through my research journey. They were always available to help whenever I had misunderstandings or needed guidance in my practice.

Another researcher I would like to acknowledge is Tebogo Tsekeli, a PhD student in my research group. He played a significant role in my research journey by aiding in getting to understand the materials studied since they are his research field. The University of the Witwatersrand is the institution I would also acknowledge for allowing me to conduct my studies on their premises, especially the school of Chemistry for allowing me access to their laboratories to run my practicals.

Finally, I want to acknowledge National Research Fund for granting me the bursary that allowed me to pursue my MSc degree and further my studies.

Abstract

Fossil fuels used as the conventional energy source play a substantial negative role in climatic changes and global warming. Their reservoirs on earth keep getting constrained, thus limiting their reliability. These issues make renewable energy sources an excellent alternative due to their abundance, environmental safety, affordability, and renewability. However, renewable energy is subjected to geographic limitations, and some sources are intermittent, which can be solved by applying energy storage devices. Asymmetric hybrid supercapacitors are an excellent choice due to the safety of aqueous electrolytes, exploitation of abundant metals in the metal oxides used, improvement of power and energy density and simple assembly and application.

In this work, manganese-rich nickel-manganese-cobalt (MR-NMC) was studied and applied in asymmetric hybrid supercapacitors as a cathode material, and reduced graphene oxide (rGO) was used as an anode. Synthesis was done using co-precipitation-(Conv), laminar Taylor vortex flow reactor-(Lam), and microwave irradiation-(MW) approaches. Physical characterization was performed using XRD and TEM. Electrochemical studies were done using CV, GCD and EIS.

Three full cells/two electrode systems were assembled and studied. Those cells were rGO//Conv MR-NMC, rGO//Lam MR-NMC and rGO//MW MR-NMC. The data obtained from electrochemistry tests was used for the calculations of specific capacitance, energy and power densities. rGO//MW MR-NMC cell had the highest specific capacitance response compared to rGO//Conv MR-NMC and rGO//Lam MR-NMC over the entire current density range used, where at the current density of 0.2 A g^{-1}, rGO//MW MR-NMC had 44.77 F g^{-1}, followed by rGO//Lam MR-NMC with 15,89 F g^{-1}, then rGO//Conv MR-NMC with 13.68 F g^{-1}. There was no significant difference in the specific capacitance responses of rGO//Conv

MR-NMC and rGO//Lam MR-NMC. rGO//MW MR-NMC also exhibited higher energy density for the entire range of power density over rGO//Conv MR-NMC and rGO//Lam MR-NMC. At the power density of 678,08 W kg^{-1}, rGO//MW MR NMC had a specific energy density of 65 Wh kg^{-1}, followed by rGO//Lam MR NMC with 23.45 Wh kg^{-1}, then rGO//Conv MR-NMC with 19.82 Wh kg^{-1}. Overall, the electrochemistry and the calculated perimeters thereafter showed that microwave irradiation is a reliable approach that can be used in the preparation of metal oxides used in energy storage devices for the improvement of electrochemical performance, which potentially enables the commercialization of these systems and management of energy crisis in South Africa, Africa and the world as a whole, hence the rGO//MW MR-NMC material performed better than the other two.

Contents

Declaration i
Dedication ii
Acknowledgements iii
Abstract iv
List of figures: viii
List of tables: xiii
List of abbreviations xiv
Chapter 1 1
Introduction 1
1.1 Background and motivation of the research 1
1.2. Problem statement 5
1.3 Energy storage devices 5
1.4 Aim and objectives 14
1.4.1 Aim 14
1.4.2 Objectives 14
1.5 Dissertation outline 14
Chapter 2 16
Literature review 16
2.1 Energy storage systems 16
2.2 Supercapacitors 16
2.3 Constituents of supercapacitors 16
2.4 Types of supercapacitors 17
2.4.1 EDLC 18
2.4.2 Pseudo-capacitance 19
2.4.3 Symmetric supercapacitors 19
2.4.4. Asymmetric supercapacitors 20
2.4.5 Hybrid supercapacitors 20
2.4.6 EDL supercapacitor theoretical modelling 21
2.5 LMR-NMC 24
2.6 Synthesis approaches for producing manganese-rich nickel-manganese-cobalt (MR-NMC) materials 26
2.6.1 Chemical co-precipitation method (Implemented for conventional approach) 26
2.6.2 Laminar flow approach 27
2.6.3 Laminar flow reactor 30

2.6.4 Microwave-assisted synthesis 31
Chapter 3 34
Methods and materials 34
3.1. Conventional and Laminar MR-NMC 34
3.1.1. Materials used 34
3.2 Material characterization 36
3.3 Electrochemical characterization 37
Chapter 4 38
Results and discussion 38
4.1 Physicochemical characterization 40
4.2 Electrochemical characterization 45
Chapter 5 58
Conclusion and recommendations 58
Future work 59
REFERENCES 61

List of figures:

Figure number	Figure name	Page number
1.1	A schematic illustration of the greenhouse effect	2
1.2	Renewable energy map 2050: The use of renewables in total final energy consumption terms	4
1.3	Ragone plot illustrating the power and energy densities of different energy storage technologies: Capacitors, electrochemical capacitors, batteries, and fuel cells	7
2.1	A schematic representation of the constituents of an electrochemical supercapacitor	17

2.2	Schematic illustration of (a) EDLC; (b) Pseudocapacitance; (c) Symmtric superapacitor, (d) Asymmetric supercapacitor; (e) Hybrid supercaacitor	18
2.3	Helmholtz's EDL model	21
2.4	Gouy's EDL model	23
2.5	Schematic representation of layered LMR-NMC	24
2.6	Schematic representation of the cylindrical Taylor Couette system	28
3.1	Schematic representation of the synthesis of MR-NMC (For laminar approach, the centrifuge is replaced with a laminar reactor)	36

4.1	XRD patterns of the as-synthesized samples	41
4.2	TEM images of the as-synthesized samples	43
4.3	(a) Schematic representation of a hybrid supercapacitor made of rGO and MR-NMC, (b)Cv of rGO and MR-NMC combined to form overall CV of the hybrid supercapacitor, (c) CV plots of rGO//Conv MR-NMC, rGO//Lam MR-NMC and rGO//MW MR-NMC, (d) GCD of rGO//Conv MR-NMC, rGO//Lam MR-NMC and rGO//MW MR-NMC, (e) Current density vs specific capacitance of rGO//Conv MR-NMC, rGO//Lam MR-NMC and rGO//MW MR-NMC	47

4.4	(a) Nyquist plots of rGO//Conv MR-NMC, rGO//Lam MR-NMC and rGO//MW MR-NMC hybrid supercapacitors (insert, electrical circuit used to fit the impedance data), (b) Bode plot of rGO//Conv MR-NMC, rGO//Lam MR-NMC and rGO//MW MR-NMC hybrid supercapacitors, (c) real capacitance, C′ and (d) imaginary capacitance, C″ with frequency for rGO//Conv MR-NMC, rGO//Lam MR-NMC and rGO//MW MR-NMC hybrid supercapacitors	52
4.5	(a) Power density vs energy density of the three assembled full cells, (b) Coulombic efficiency of the three assembled full cells	54

List of tables:

Table number	Table name	Page number
4.1	EIS results of rGO//Conv MR-NMC, rGO//Lam MR-NMC and rGO//MW MR-NMC hybrid supercapacitors	50
4.2	Comparison of maximum energy densities of other asymmetric hybrid supercapacitors and asymmetric supercapacitors studied in this work	56

List of abbreviations

AC	Activated carbon
Co	Cobalt
Conv	Conventional
CPE	Constant phase element
CV	Cyclic voltammetry
EDL	Electric double layer
EDLC	Electric double layer capacitance
EES	Electrical energy storage
EIS	Electrochemical impedance spectroscopy
GCD	Galvanostatic charge-discharge
GDP	Gross domestic product
Kw/kg	Killowatt per kilogram
Lam	Laminar
Li	Lithium
LIB	Lithium-ion batteries
LMR-NMC	Lithium-manganese-rich nickel-manganese-cobalt
mAh/g	Milli Ampere hour per grams
ml	Millilitre
Mn	Manganese

MR-NMC	Manganese-rich nickel-manganese-cobalt
MW	Microwaved
NDP	National domestic product
Ni	Nickel
NMP	N-methyl pyrrolidinone
PVDF	Polyvinylidene fluoride
pVp	polyvinylpyrrolidone
rGO	Reduced graphene oxide
SEI	Solid electrolyte interface
SEM	Scanning electron microscopy
TEM	Transmission electron microscopy
TM	Transition metal
Wh/kg	Watt hour per kilogram
XRD	X-ray diffraction

Chapter 1

Introduction

This chapter focuses on the background and motivation of the research. It covers reasons that motivated the choice of the field of research as well as the significant benefits that would result.

1.1 Background and motivation of the research

The world predominantly relies on fossil fuels as a conventional method to produce electrical energy [1,2]. Due to a significant increase in the global population growth rate, there has been a rise in the demand for more electrical energy for use in households, transportation, industries, and other essential sectors to make the lives of human beings more manageable and flexible [3-5]. This has caused excessive use of fossil fuels, thus increasing greenhouse gas emissions. As it is a familiar concept, these gases threaten the well-being and safety of the environment and humans by being the leading cause of thermal pollution, global warming, and climate change [6]. Emission of greenhouse gases causes air pollution that affects humans and living organisms when they inhale polluted air, and this would lead to a high mortality rate of humans as well as a collapse in the food chain of the environment, thus affecting the natural energy cycle [7-12].

Figure 1.1 below depicts an illustration of the greenhouse effect as it also highlights some of the leading gases responsible for the emergence of the impact.

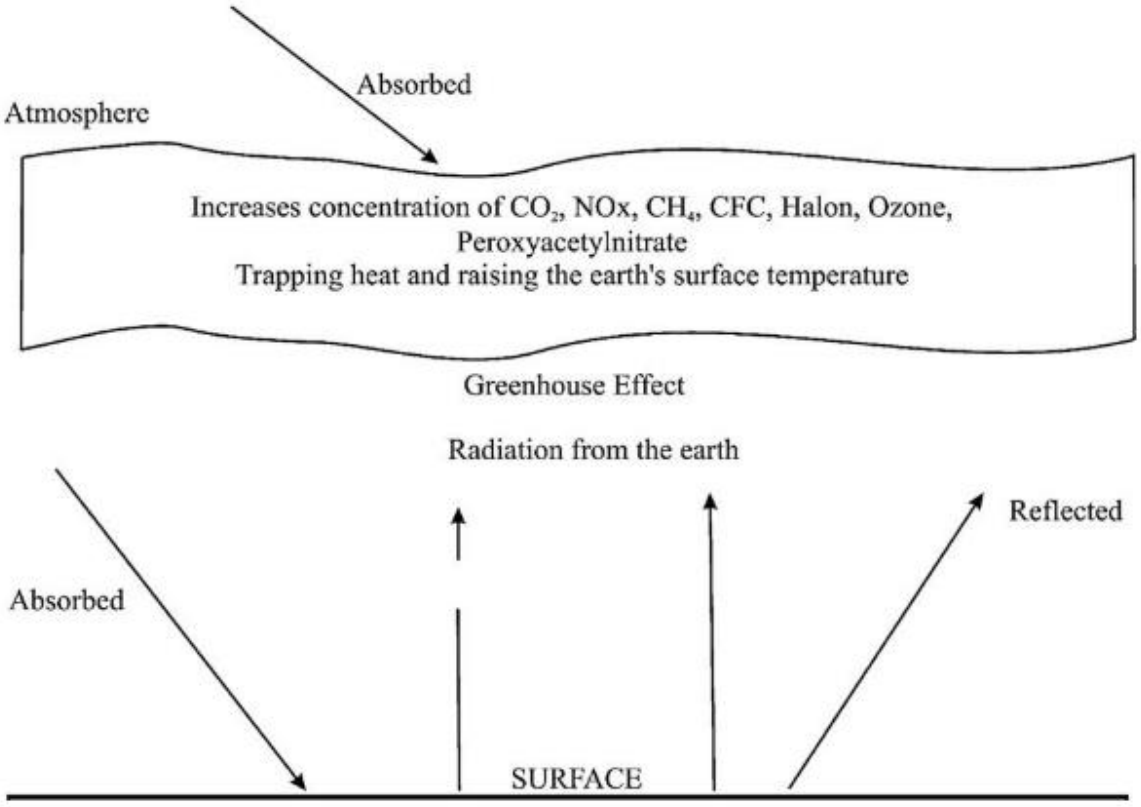


Figure 1.1: A schematic illustration of the greenhouse effect [1]

The negative impact that fossil fuels have caused over the previous years, in the present time, and the potential impact in the future have raised concerns about relying on them for further production of electrical energy [1]. Due to this, renewable energy source alternatives have been applied to provide affordable, sufficient, and environmentally friendly energy that does not threaten the environment and humans. The consequences of fossil fuels have made alternative renewable energy sources an urgent requirement for such a growing and ever-changing world [13].

Some reliable renewable energy sources include solar, wave and wind energy. The advantage of the application of these alternatives is that their sources are natural; thus there would be

constant, reliable, abundant, and non-constrained sources of the necessary feeds for the provision of energy, and the sources do not subject nature and humans to unbearable levels of danger, unlike fossil fuels.

Renewable energy sources have been identified to possess the tremendous potential of efficient energy supply soon over fossil fuels, also because fossil fuel reserves have constantly declined as these materials have been mined for many decades. The shift from fossil fuels is also inspired by the goal to limit the average global temperature increase to 2 ^{o}C [14,15]. It is believed that this would be achieved if there were renewable energy sources with the potential to meet the energy demands now and in the future. Geothermal heat as an energy source has exhibited higher energy production estimates in the future, making it a credible source. The hottest deserts in the world cover more than 10 million km^2, creating the possibility of constructing large solar energy farms that would lead to the harvesting of abundant sunlight to convert into electrical energy that would meet the level of energy demands globally [14].

D. Gielen and colleaques [15] reported the significant role that sustainable energy sources play in achieving the goals highlighted in Agenda 2030. As highlighted on their paper, this agenda was adopted by the United Nations General Assembly's Sustainable Development Goals in 2015. The motion focuses on eradicating poverty, dismantling inequality and injustice, and protecting the planet's environment. There is an urgent need to shift from the utilization of fossil fuels because the emitted Carbon dioxide that is energy-related makes up two-thirds of the total greenhouse gases. There has been a notable growth in energy generation from renewable sources, including solar. In 2017, more than 60% of all new electricity capacity was attributed to renewable sources. Also, electricity from renewable sources has been reported to have lower costs than fossil fuels, enhancing affordability and access. Analysis has shown that CO_2 emission intensity needs to be reduced by 85% between 2015 and 2050, which brings

forth the significance of renewable energy sources. The shift into renewable energy sources can potentially create about 19 million jobs.

Figure 1.2 depicts the deployment of renewables to indicate their importance in energy production [15].

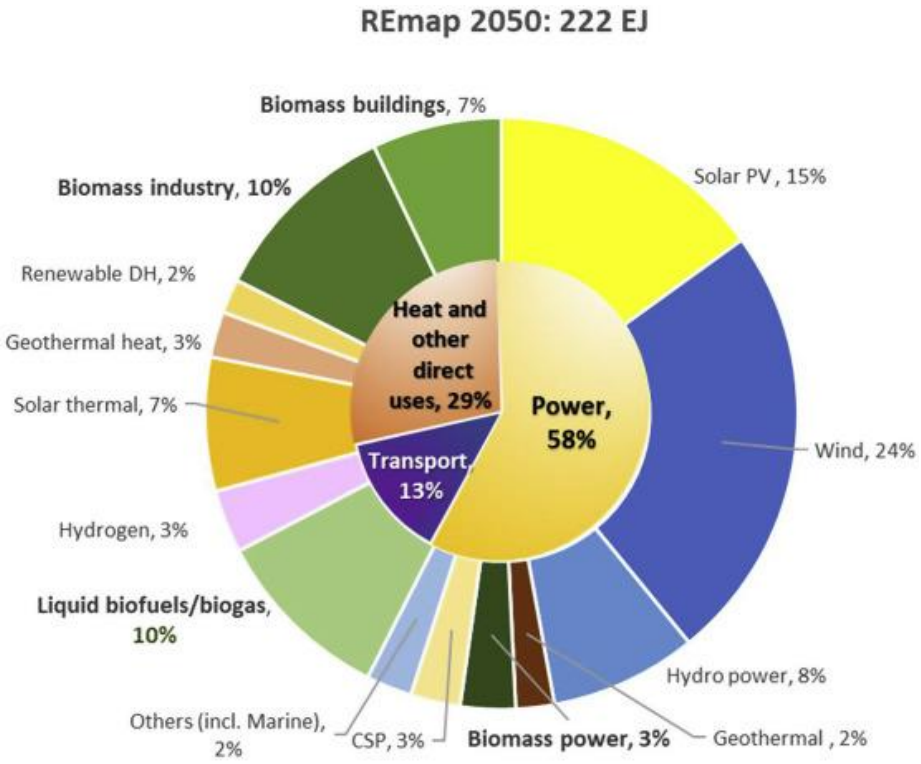


Figure 1.2: Renewable energy map 2050: The use of renewables in total final energy consumption terms [15]

The major issue with renewable sources of electricity production is that they are intermittent [14]. Therefore, they pose the challenge of constant supply of electrical energy. This introduces a gap between energy production and sufficient energy supply. What fills in that gap is energy storage devices. There has been extensive research on energy storage systems as an attempt to dismantle electrical energy supply issues [16-18]. Amongst these systems, batteries and supercapacitors have received so much attention for the use of storing electrical energy generated from renewable resources [19, 20].

1.2. Problem statement

The unavoidable consequences of fossil fuels to the environment and human health lead to the need for implementation of renewable energy. Due to renewable energy sources being intermittent, energy storage systems play a significant role in ensuring that there is enough supply of electrical energy that meets people's demands and also mitigate the negative impacts of generation of electrical energy from fossil fuels. Therefore, more focus should be invested into studying energy storage materials, improving their performance to ensure that they perform in the best possible way to be an alternative or a substitute to the conventional way of electrical energy generation (i.e. Fossil fuels).

1.3 Energy storage devices

Energy storage devices hold significant importance in balancing the demand and supply of electrical energy. If these devices are developed in a way that they can store high levels of energy, there might be an emergence of flexibility and sufficient reliability of the grid performance. Since these systems enable large-scale provision of energy through renewable energy sources, there would be minimal energy demand due to sufficient supply of energy stored in large quantities. With the conventional energy source, there are power breakouts from time to time, this becomes quite an inconvenience to sectors that require a constant supply of electrical energy, industries as an example would be slowed down, which would negatively affect the economic cash flow, with energy storage devices developed efficiently with improved performance, there would be storage of sufficient energy that mitigates and minimizes the impact of power breakouts. Some of the energy storage technologies applied are supercapacitors, fuel cells and batteries [21].

If the energy produced from renewable energy sources is directly supplied to sectors that require electrical energy, there would be an over-production of energy that ends up being lost, leading to an inefficient supply of energy, and thus keeping demand on a significantly higher level. In most cases, the lost energy is not even recovered. This proves the significance of investing attention into energy storage systems that are reliable and have the potential to minimize such consequences and raise energy production efficiently. When energy storage systems are applied, there is a separation of production and consumption, this brings forth the ability to produce sufficient energy before supply so that inefficiency can be avoided. These systems also hold the potential of revolutionizing the global industry by generating high levels of revenue in business [13]. This would be an advantage in the fact that countries that invest in this technology would generate higher gross domestic products (GDP) and national domestic products (NDP), together with job creation locally and globally, thus reducing the levels of poverty and unemployment worldwide. Supercapacitors have received a wide range of attention as a solution to the need for reliable and sustainable energy storage technologies. Due to the high current that they can operate with, they are an excellent alternative to standard electrochemical batteries that have been in the commercial market over the past years to now. Another reason for the application of this technology is that it can be applied when there is a need for storage or release of electrical energy in a brief period, making this technology time efficient [22].

Since this technology has the potential to bridge the gap between batteries and conventional capacitors, it can be applied in hybrid electric vehicles, electric vehicles, fuel cell vehicles, trains, trolley buses and electronic devices with mitigated chances of interruption in power supply [22].

This energy storage system exhibits excellent power density as shown on the Ragone plot in **Figure 1.3** (Which also emphasizes the fact that supercapacitors fill the gap between

conventional capacitors and batteries), good reversibility, long cycle life and enhanced intrinsic safety as compared to other known and commercialized energy storage technologies, mainly batteries [23].

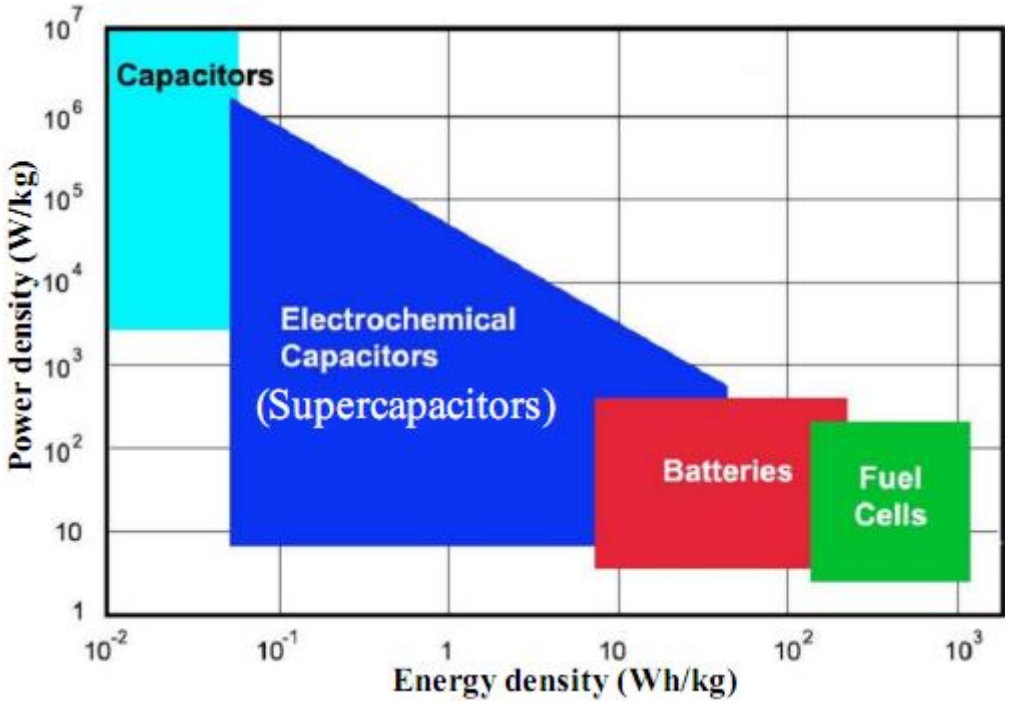


Figure 1.3: Ragone plot illustrating the power and energy densities of different energy storage technologies: Capacitors, electrochemical capacitors, batteries, and fuel cells [22]

Compared to batteries and fuel cells, supercapacitors exhibit long charge-discharge cycles and wide operational temperature ranges [24], making them an excellent energy storage technology in the sense that they can store more electrical energy for a longer time, supply that power for more extended periods and retain their stability even at higher temperatures, meaning they have high thermal stability.

In exploring supercapacitors, hybrid supercapacitors have been received as the best option. This is due to their combination of electric double-layer capacitance (EDLC) and pseudo-

capacitance [25]. As a result, it improves the technology's electrochemical performance, thus leading to high capacitance. The hybrid system exploits the charge storage mechanism of an EDLC material and that of a pseudo-capacitive material, thus improving the power, energy density, and overall capacitance. This ensures that hybrid supercapacitors become the best alternative to other energy storage devices. Electrochemical capacitors exhibit excellent power density due to the faster charge mechanism associated with the double-layer capacitance; this mechanism occurs on the interface between the electrode of the capacitor and the electrolyte. Due to this, the electrochemical performance of hybrid supercapacitors surpasses that of batteries [26]. The diffusion kinetics constrain rechargeable batteries' version, which limits their charging and discharging rate and power density. Unlike these technologies, hybrid supercapacitors can store large amounts of charge at high power rates [24].

In the exploration of cathode materials used for energy storage devices, NMC cathode materials have gained more attention as potential candidates. These materials have been widely used in Li-ion batteries, with a variation of the amounts of Li, Ni, Mn, and Co metal ions to exploit the advantages of integrating the mentioned ions for the formation of NMCs and evaluate how the synergy of those ions might affect the overall electrochemical performance of the cathode material.

The reason why these materials have gained so much interest is that they have exhibited high energy densities, great structural stability, improved safety, and low cost since they are the result of the incorporation of cheaper transition metal ions [27].

These materials provide the merits of metal oxides which are $LiCoO_2$, $LiMn_2O_4$ and $LiNiO_2$. In this combination, NMCs display high energy density which can be attributed to $LiCoO_2$, high thermal stability, which is due to $LiMn_2O_4$, and high reversible capacity which is caused by the presence of $LiNiO_2$ [28]. The materials have an excellent theoretical capacity of 270

mAh g^{-1} [29]. The hexagonal α-$NaFeO_2$ structure with *R3m* space group has been reported to be the cause of NMC high theoretical capacity [28].

NMC materials have fast Li^+ ion transfer and movement of electrons [29], thus improving the capacitance, rate capability and cyclability. The improved kinetics of these materials can be attributed to their open framework [28]. The open framework maximizes the contact area between the cathode material and the electrolyte even at higher current densities, thus leading to improved kinetics and ion migration together with improved reactivity on the cathode, by minimizing overall reaction times. NMC materials have the potential for mitigation of the drawbacks that occur because of the presence of a Solid-Electrolyte Interface (SEI) [28].

In NMCs, the electrochemical inactivity of tetravalent manganese plays a significant role in the stability of the materials, thus preventing capacity fading induced by Mn dissolution. Cobalt on the other hand reduces cation mixing, this prevents the formation of charge in the structure of the cathode material. Nickel ions are largely involved in the redox reactions that are vital for energy storage [30].

Ni ions present in the NMC have a significant impact in the cycling capacity of an energy storage technology, and this happens at the voltage range of 3.0 V- 4.2 V, this happens as the valence of Ni ion changes from Ni^{2+} to Ni^{4+} [31]. The voltage range mentioned is quite high, thus providing the possibility of excellent electrochemical performance.

N. Kiziltas [31] and colleagues evaluated the electrochemical performance of an NMC cathode material synthesized using the sol-gel method with table sugar as a chelating agent. The synthetic method was reported to cause good cation distribution. The electrochemical tests were performed at 0.1C-rate in the voltage range of 3.0 V – 4.2 V. The first discharge capacities were 166 and 149 mAh g^{-1}. On the 10^{th} cycle, the capacities changed to 146 and 144 mAh g^{-1}, with 96.5 % Coulombic efficiency. The sample here performed better than the commercialized

NMC from Tanaka [31]. Therefore, the use of a synthetic method that improves the distribution of cations can improve the electrochemical performance of NMC materials.

Amongst these NMC cathodes, LMR-NMC materials have received more attention and are considered the best alternative over Nickel rich NMCs, which have been relied on for application in energy storage systems due to their intrinsic very high energy density at the cell and battery pack level [32, 33]. Ni-rich NMCs cannot be implemented and commercialized on a larger scale because there is the formation of highly reactive Ni^{4+} at the delithiated state, which leads to unfavourable side reactions with the electrolyte. Also, when Ni^{4+} is reduced, it causes the formation of Ni-O impurity phase and Oxygen loss on the material's surface, which as a result damages the crystal structure and thus reduces the cycling and thermal stabilities of Ni-Rich NMCs [34].

Although this material has exhibited excellent attributes that make it a preferable cathode over other researched materials, it has shown several drawbacks that hinder it from being used on a large scale and commercial level.

There are two main issues that limit the application of this material, which are capacity fade and voltage decay during electrochemical cycling [35]. Another undesirable issue that the material faces during cycling is the occurrence of high irreversible capacity at high voltages [36]. These occurrences bring the need to introduce solutions with the goal of making the material more competitive, especially when the material's benefits for energy storage technologies are highly significant to ignore.

Voltage decay holds a high potential to reduce the energy density of the material since the cell voltage exhibits direct proportionality with the cell's energy. This phenomenon also compromises the material's state of charge determination, which in return complicates the management of energy storage technologies [37].

Voltage decay and capacity fading of the material are a consequence of the structural transition of NMC from its layered form to a spinel structure during cycling [38]. Prior to structural transformation, there is an activation of Li_2MnO_3 into an active MnO_2 species. This activation process leads to the release of oxygen in the form of Li_2O. The released oxygen participates on a side reaction with the cathode material, thus leading to unwanted phase transformation. The side reaction happens when the energy storage system is charged to 4.8 V [39].

The formation of the domain spinel structure from the layered structure occurs due to migration of transition metals of NMC cathode material from the transition metal layer to the Li-layer. During this migration, it's mostly Ni ions that are involved compared to Mn and Co [36].

In other words, there are rearrangements of transition and alkali ions, thus the inducement of phase transformation, and the most problematic issue with this phenomenon is that the phase transformation is irreversible [40]. This means that if there is no solution introduced to this problem, the material's electrical performance can be limited throughout further cycling.

During cycling at high voltages, there is a decomposition of salt and solvent, and their decomposition products deposit on the surface of the cathode material, this increases the impedance of the material and thus causing a drop in the capacity [38]. What causes the increased impedance is the formation of a thick solid-electrolyte interface film (SEI) that hinders the penetration of Li^+ into and out of the cathode material.

There is a dissolution of transition ions such as Mn from the cathode material which also results in significant capacity fading [38]. When these ions get off the material, structural integrity and stability are compromised, leading to poor electrochemical performance during cycling. In other words, there is poor cycling stability when the material's structural integrity is weakened by the dissolution, thus causing poor capacity/capacitance retention.

There are possible side reactions that occur between the active cathode material and the electrolyte, these reactions lead to poor rate capabilities and bad cyclabilities [30]. This is because the reactions introduce severe physical and electrochemical changes that render the material less electrochemically active. For example, the occurring side reactions might inactivate the material's ions that take part in the redox reactions that are significant for energy storage.

LMR-NMC cathode material has been applied in lithium-ion batteries extensively. However, it is not the focus of interest due to the drawbacks that have been covered previously. Some of the further disadvantages of further exploring lithium-rich materials are as follows: Lithium-ion batteries have been utilized as energy sources of portable devices which dates from the year 1991, which is the year they were commercialized. The reliance on these systems emerged from their high energy density, cycle life and electrochemical rate [41-47]. However, there is currently a concern associated with the reliance on lithium-based materials for energy storage devices. This is because these systems are known for their poor safety from the highly volatile lithium-ion which could be problematic if lithium is abundant/excess in the material used, lower lifetime, poor low-temperature performance and high cost. Also, the lithium metal natural reservoirs have become constrained due to excessive use of the metal. These issues limit the wide-scale commercialization of lithium-ion-based systems [48, 49].

On the other hand, manganese-rich NMC is of significant interest for application as a cathode material in energy storage systems. The first reason is that this material has not been widely explored in research for its application in energy storage, this opens a field of exploring its advantages and enhancing them through different methods to improve its electrochemistry.

South Africa is known for having an abundance of manganese metal. Due to this, there can be an excess supply of this metal to prepare MR-NMC that can be applied in energy storage

systems. This would balance the demand and supply gap of electrical energy via energy storage systems and play a positively significant role in the upscaling and commercializing of these systems. Also, the high availability of manganese in the country reduces the cost of the materials based on this metal, thus making energy storage systems based on this metal more cost-effective.

The scarcity of lithium increases the cost. When we also consider the cost and safety issues associated with the alternative of LMR-NMC which is Ni-Rich NMC, there is a need to shift from expensive metals to affordable and abundant ones, and that is manganese, this is why the increase of manganese content in NMC material deserves significant consideration in the field of energy storage material research [50]. This would be a vital approach to the energy crisis provided that the material reaches energy and power density levels that match those of Ni-Rich and LMR-NMCs.

1.4 Aim and objectives

1.4.1 Aim

This research study aimed to test MR-NMC cathode materials synthesised using different methods for hybrid supercapacitors.

1.4.2 Objectives

The objectives of this research study are as follows:

- Synthesise MR-NMC cathode materials using co-precipitation-(Conv), laminar Taylor vortex flow reactor-(Lam) and microwave-(MW) irradiation method.
- Physical characterization of MR-NMC cathode materials using XRD and TEM.
- Assembly of hybrid full cells using MR-NMC materials and reduced graphene oxide (rGO).
- Evaluate the MR-NMC cathode materials in a three-electrode system using cyclic voltammetry.
- Investigation of electrochemical performance of rGO//Conv MR-NMC, rGO//Lam MR-NMC and rGO//MW MR-NMC hybrid supercapacitors in a two-electrode system using cyclic voltammetry, galvanostatic charge/discharge and electrochemical impedance spectroscopy.

1.5 Dissertation outline

The following are the chapters that make up this dissertation:

Chapter 1: Introductory chapter giving the research background, motivation, aim and objectives of the study.

Chapter 2: Focuses on the literature review of energy storage systems. Specifically supercapacitors, the types of supercapacitors, the working mechanisms, the materials of interest and the synthetic approaches followed.

Chapter 3: Presents the experimental approaches followed, which features the materials used and the characterization techniques used.

Chapter 4: Focuses on the results and discussion of Conv MR-NMC//rGO, Lam MR-NMC//rGO and MW MR-NMC//rGO asymmetric hybrid supercapacitors.

Chapter 5: This is a concluding chapter that summarises the results of the study and also presents the recommendations that can be applied in future to improve the quality of the study and the performance of the materials studied.

Chapter 2

Literature review

2.1 Energy storage systems

There is an increase in energy demand all over the world. This phenomenon has led to the development of environmentally friendly and efficient energy storage systems. Amongst these energy storage systems, electrochemical systems have been deemed as the best options to solve the energy crisis. Such systems feature batteries, fuel cells and supercapacitors [51]. Amongst these energy storage systems, supercapacitors have come forward as the best option due to their excellent performance in power density, response time and the systems being long-lasting [52].

2.2 Supercapacitors

Supercapacitors have proven to be a significant improvement from conventional capacitors, thus making them one of the noble focuses in energy storage systems. Conventional capacitors store energy via static charge. The capacitor is charged through the application of potential on the positive and the negative electrodes of the system. What makes supercapacitors better than conventional capacitors is that the former provides very high capacitance. These devices are an excellent option for energy storage that is subjected to charge and discharge cycles at high currents and short durations [53]. Supercapacitors are electrochemical capacitors that have the potential to store significantly high amount of energy and discharge it at rates required for the application [54].

2.3 Constituents of supercapacitors

Figure 2.1 shows the constituents of electrochemical supercapacitors and their arrangement to illustrate how they are integrated for the functioning of these energy storage systems.

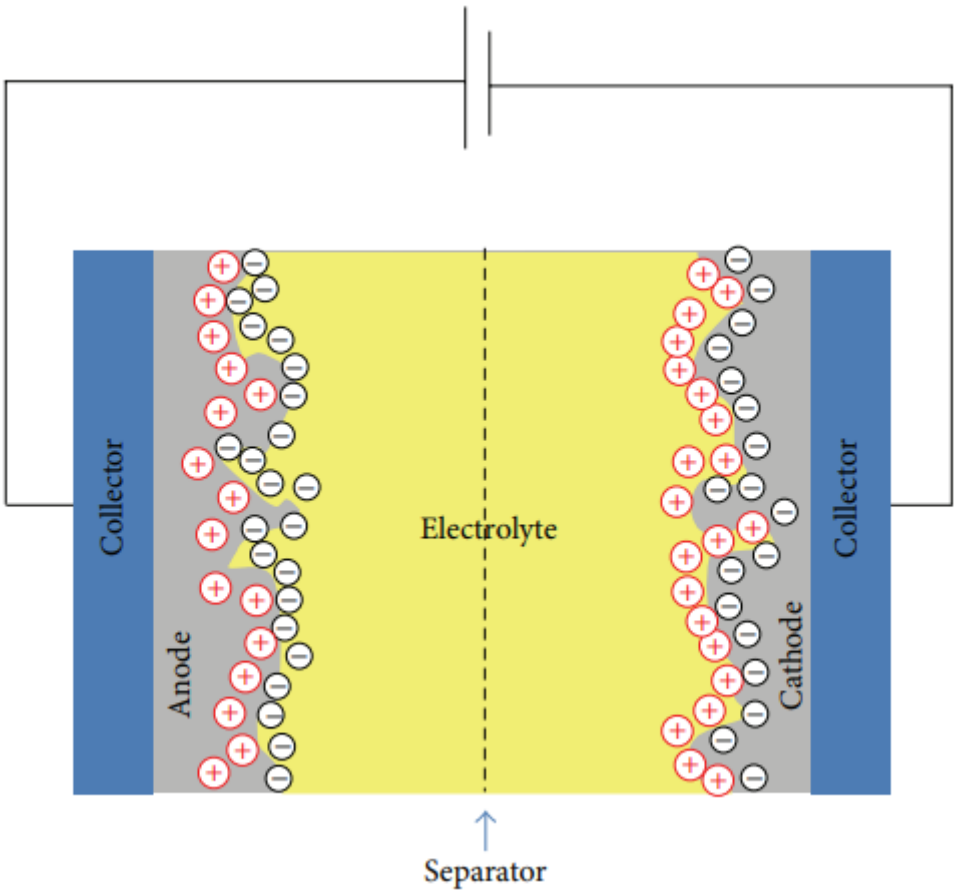


Figure 2.1: A schematic representation of the constituents of an electrochemical supercapacitor [55]

The components of this technology are like those of conventional metal ion batteries. Supercapacitors are composed of two electrodes (negative and positive) kept apart by a separator. These components are immersed in an electrolyte. The cathode material is coated on the selected current collector. The separator should be permeable concerning the electrolyte applied to permit the migration of ions between the two electrodes involved during charge-discharge processes. Hybrid supercapacitors exploit both EDLC and pseudo-capacitance energy storage mechanisms, and it is significant to understand how these two energy storage mechanisms work.

2.4 Types of supercapacitors

Figure 2.2 below provides illustrations of different supercapacitors and simultaneously displays the mechanisms that accompany charge storage in the respective supercapacitors. The sections that follow explain each mechanism.

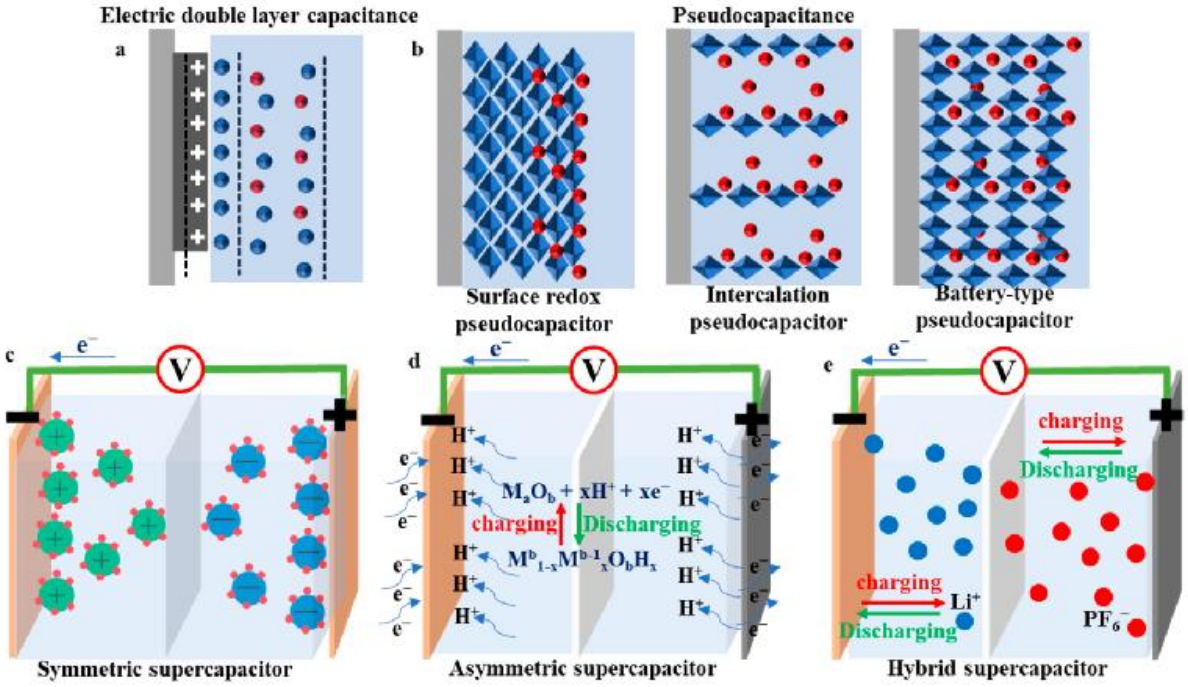


Figure 2.2: Schematic illustration of (a) EDLC; (b) Pseudocapacitance; (c) Symmtric superapacitor, (d) Asymmetric supercapacitor; (e) Hybrid supercaacitor [56]

2.4.1 EDLC

In EDLC capacitance, it is the separation of electronic and ionic charges at the interface between the electrode and the electrolyte solution, that is responsible for energy storage. The capacitance in this system is a result of a non-faradaic storage mechanism, there is only physical charge transfer involved [57].

The most significant feature in EDLC capacitance is the surface area of the electrode used [58]. Therefore, a high surface area electrode is needed for efficient accessibility by the electrolyte for excellent electrostatic charge storage mechanism to occur.

2.4.2 Pseudo-capacitance

On the other hand, pseudo-capacitance charge storage mechanism is the opposite of EDLC charge storage mechanism. In this system, energy storage is brought forth by reversible redox reactions of the active electrode material used [59]. Since redox reactions are significant, materials that permit intercalation and de-intercalation of ions can be explored for the exploitation of the pseudo-capacitance they can offer.

In this system, oxidation occurs on the cathode, where the resulting ions from the active electrode material travel with the aid of the electrolyte through the separator to the anode where reduction occurs. These two reactions are the ones responsible for charge storage. Faster and reversible redox reactions are fuelled by the application of potential on the system, thus generating charges which are stored in the end [58].

Supercapacitors can also be classified into symmetric, asymmetric and hybrid supercapacitors based on the composition and nature of the electrodes applied. The following section highlights the differences in the three mentioned types of supercapacitors.

2.4.3 Symmetric supercapacitors

Briefly, symmetric supercapacitors are constituted of a combination of identical materials that share similar physical and chemical properties and have the same capacitance at both the negative and positive electrodes. In other words, the two materials applied should either have an EDLC charge storage mechanism or the mechanism of pseudocapacitance, not both charge storage mechanisms being involved [60].

2.4.4. Asymmetric supercapacitors

On the other hand, asymmetric supercapacitors are composed of two different electrode materials where one functions as a cathode and the other function as an anode. These materials provide different charge storage mechanisms [61]. In these types of supercapacitors, the working potentials of two different electrodes can be explored, thus providing the opportunity to have an overall large potential window for the supercapacitor.

2.4.5 Hybrid supercapacitors

These systems function through the combination of EDLC and pseudo-capacitors, thus there is a guaranteed enhancement in the energy density. Considering that electrochemical supercapacitors exhibit poor energy density; hybrid supercapacitors fill in the gap using a capacitor electrode and a battery-like/battery-based electrode that compensates for the need for high energy density considering that batteries offer high energy density. The hybrid also leads to high working voltage [24]. This in return optimizes the overall electrochemical performance of hybrid supercapacitors and thus leads to excellent overall capacitance which is the combination of EDLC and pseudo-capacitance.

There are two charge storage mechanisms that are responsible for the overall capacitance of a hybrid supercapacitor. The cathode electrode is battery-like. Therefore, cathode materials used in metal-ion batteries can be exploited for the capacitive advantages they have to offer. The anode electrode is that of a capacitor. Preferably one that offers a high surface area.

The following section focuses on the theoretical modelling of EDL supercapacitors to explain charge storage mechanism between electrodes and electrolytes. Figures are also provided to vividly explain the processes that occur during charge storage.

2.4.6 EDL supercapacitor theoretical modelling

It was Helmholtz who discovered how charge storage mechanism occurs on the interface between the solid electronic conductor and the liquid ionic conductor in 1853. When voltage is applied to the system, there is formation of a space charge at the interface, this is due to the electrostatic influence present. This space charge is known as electric double layer [62].

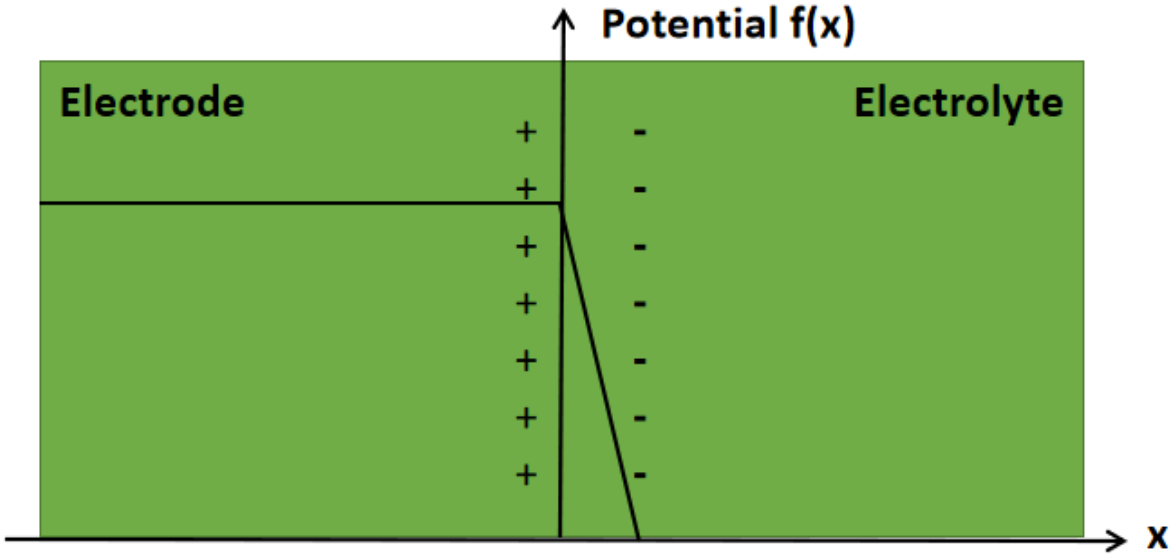


Figure 2.3: Helmholtz's EDL model

Figure 2.3 above shows the formation of the electric double layer between the electrode and the electrolyte.

From the model shown in **Figure 2.3**, capacitance(C) depends on the permittivity of the solvent/electrolyte(E) and the thickness of the electric double layer(d) which is the molecular diameter of the solvent, as shown by the equation that follows [62]:

$$C = \frac{E}{d} \quad (1)$$

The issue with the Helmholtz 'model is that it could not account for the voltage dependence of capacitance, which left a gap in the understanding of how voltage affects the capacitance of the electric double layer.

Due to this, Gouy and Chapman developed an EDL model that explains the relationship between voltage and capacitance.

According to them, capacitance across the liquid/solid interface is obtained as a function of surface potential [62]. This observation brings about the emphasis why there is a need for a high surface area of the electrode used. A high surface area tolerates and provides high potential which is directly proportional to the capacitance as seen in the mathematical equation that follows [62]:

$$C=Z.\sqrt{\frac{2q.n_o.E}{uT}}\ .ch\left(\frac{Z.\Psi_o}{2u.T}\right) \quad (2)$$

The following is what the symbols of the equation mean:

Z-Valence of electrolyte ions

n_o-Concentration of anions and cations at thermodynamic equilibrium

E-Dielectric permittivity of electrolyte

q-Elementary electric charge

k-Boltzmann's constant

T-Temperature

U_T-Thermodynamic potential unity (U_T=k.T/q)

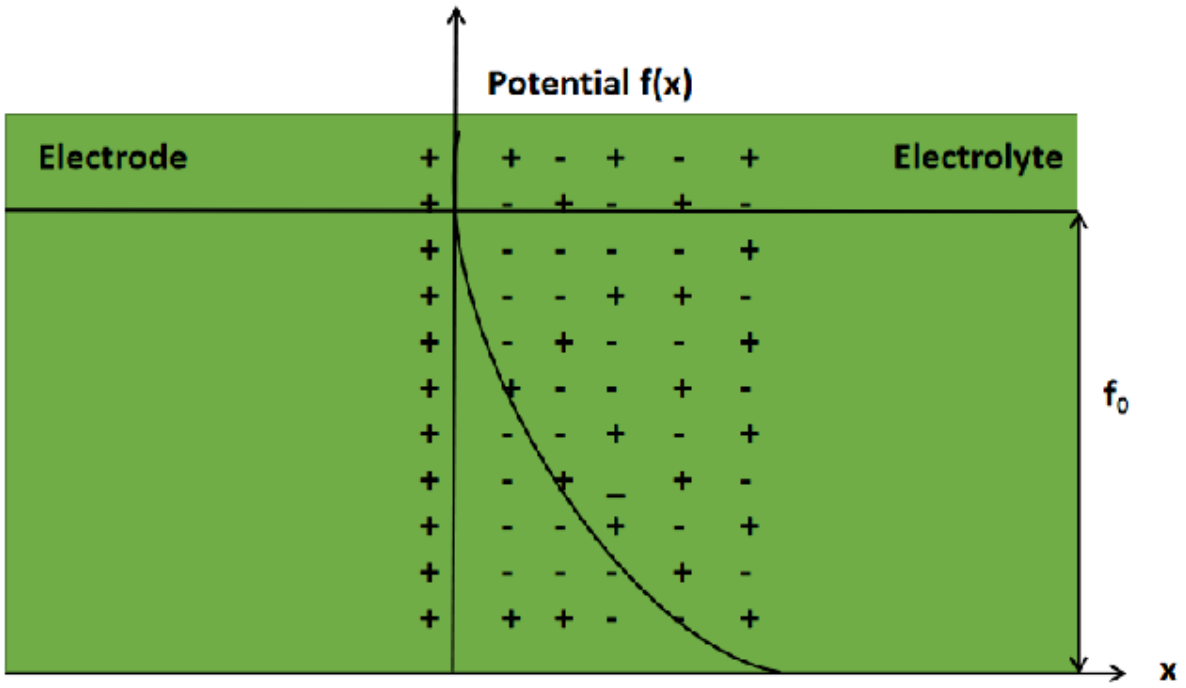


Figure 2.4: Gouy's EDL model

It is evident on **Figure 2.4** above that there is a formation of space distribution of ionic charge in the electrolyte, which leads to the formation of a diffused layer that is involved in the capacitance of electric double layer.

As the surface potential of the electrode used increases, there is an exponential increase in the surface capacitance. When the valence of the electrolyte ions increases, the rate of increase of surface capacitance is higher than when the valence is low. Also, as the concentration of anions and cations at thermodynamic equilibrium increases, surface capacitance increases significantly [62].

The following section focuses on lithium-manganese-rich NMC cathode materials to emphasize the reasons why they can be explored for application in hybrid supercapacitors.

2.5 LMR-NMC

NMC materials that are rich in lithium and manganese are an excellent option for energy storage technologies because their energy density can exceed 1000 $Whkg^{-1}$, they also exhibit high achievable reversible capacity which can be greater than 250 mAh g^{-1}. They can function in wider voltage ranges such as 2.5 V- 4.8 V. They are thermally safer than NMC-111, which is caused by low Co content [38]. All these attributes of LMR-NMC cathodes are significant in the improvement of electrochemical performance of energy storage devices, which leads to improved capacitance/capacity.

In LMR-NMC, when the content of lithium is increased, there is an enhancement of electrochemical performance, which as a result improves the material's capacity [63]. This ensures that the energy storage system that applies this material as the cathode can store high electrical energy, thus improving the possibilities of commercialization.

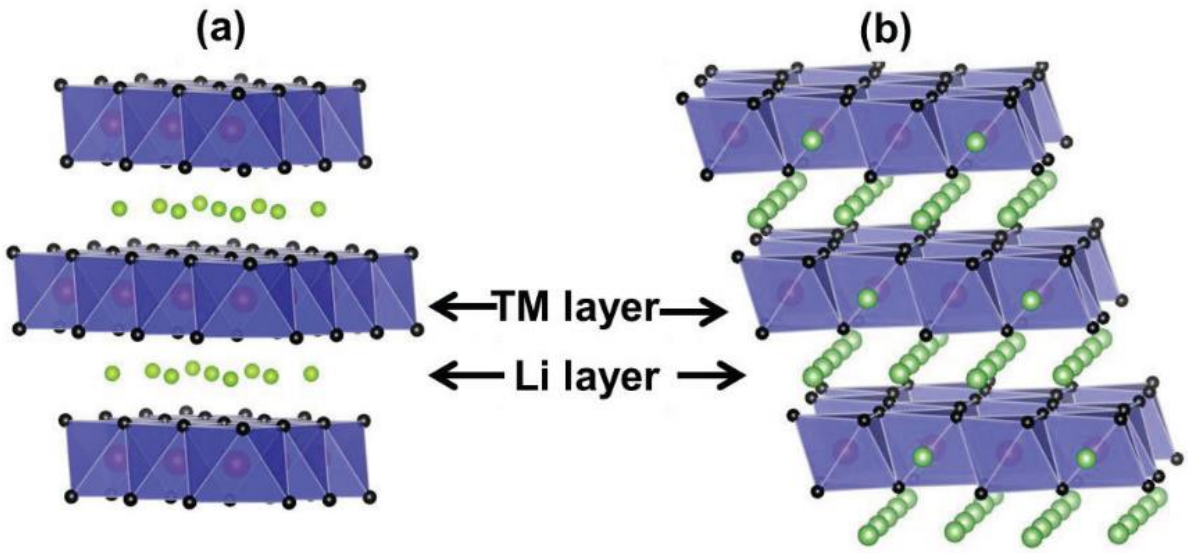


Figure 2.5: Schematic representation of layered LMR-NMC [64]

Looking at **Figure 2.5**, intercalation and de-intercalation of Li^+ ions can easily occur, this is due to the presence of large available open space between the transition metal slabs of the LMR-NMC cathode material [39]. The fairly large inter-slab distances permit fluent migration of Li^+, thus improving the kinetics associated with the material, leading to improved redox reactions as a result. The layered structure of LMR-NMC makes it an excellent material to be used for energy storage technologies.

The excess lithium ion LMR-NMC resides in the transition metal layer of the material as shown in **Figure 2.5**. The nature of cation ordering leads to the formation of a new face of the material which is Li_2MnO_3 [64]. The presence of this new phase leads to more extraction of lithium ions from the material during charging, thus leading to an improvement in the delivered capacity during application.

As it has been already highlighted in the introduction section. There has not been extensive research done on the MR-NMC material for application in energy storage devices. To the best of our knowledge, this is the first time this material is being applied as a cathode material in hybrid supercapacitors, thus there is no literature review on the material. There are reasons highlighted before as to why there is a need to explore MR-Rich NMCs rather than LMR-NMCs, generally, this is to shift away from the drawbacks that are associated with LMR-NMC, and also explore the potential advantages that can be presented by MR-NMCs.

There is a need to reduce the amount of cobalt and nickel in layered NMC cathode materials due to their cost and toxicity. One of the best strategies to achieve this is to increase the amount of manganese in NMC cathode materials. This is because Mn metal is more affordable due to their excessive global abundance which is two orders high than those of Ni and Co. Also, the biological toxicity of Mn is significantly less than that of Ni and Co. This makes Mn-Rich based cathode materials environmentally and economically preferable [65]. Thus, the move

towards Mn-Rich cathode materials deserves attention in the research of cathode materials for energy storage systems.

2.6 Synthesis approaches for producing manganese-rich nickel-manganese-cobalt (MR-NMC) materials

This section focuses on the synthesis approaches that were followed during the preparation of the materials of focus. The shynthesis approaches are chemical co-precipitation, laminar flow approach and microwave-assisted approach. The advantages of implementing these synthesis methods are also discussed.

2.6.1 Chemical co-precipitation method (Implemented for conventional approach)

There are various chemical synthesis methods that are pursued during the preparation of chemical materials. These methods include the sol-gel, hydro-thermal, combustion, thermal decomposition, micro-emulsion and co-precipitation. Among these synthetic approaches, co-precipitation is the best option for synthesis due to the advantages that it provides. Such advantages include cost effectiveness, low temperature, small particle size of the as-synthesized materials, high porosity, short preparation time, excellent chemical purity and high crystallinity [66]. When this method is implemented, there is also no need for using organic fuels, thus improving safety in the laboratory since these solvents pose a hazard threat by being flammeable, the approach is simple, and there is high chemical homogeneity [67].

When a reaction is conducted via chemical co-precipitation approach, precursors and a solvent are selected, the precursor salts should be soluble in the selected solvent. The salts are added in the solvent to dissolve and form a precursor solution. Stirring and heating is involved to improve the dissolution of the salts. A precipitating agent is then added into tolution, reacts

with the ions in the solution to form insoluble compounds. The resulting precipitate is then allowed to mature in the solution, where there is growth of precipitate particles, with formation of targeted size and morphology. After this, the precipitate is separated from the solution via filtration or centrifugation. The precipitate is washed to remove impurities. The precipitate is then dried to remove moisture and further calcinated to manipulate the properties of the materials synthesized.

In some cases, a solid-state reaction step is involved where solid materials are mixed together thoroughly without the involvement of any solvent, then, the mixture is taken to the furnace for calcination to modify the overall material properties and morphology.

2.6.2 Laminar flow approach

Taylor-Couette flow is a flow that is associated with a viscous liquid that is confined in between two cylinders. The motion of the fluid between the cylinders was developed and evaluated by Geoffrey Taylor in the year 1923 [68]. In this flow, only one or both cylinders can rotate, and both can rotate in either the same or the opposite directions [69]. This flow has been widely applied in studying primary instability, pattern formation, and transition between laminar and turbulence flow [70]. Interestingly, this flow has been demonstrated to be applicable and efficient in bio/chemical reactors, where the reactors that function under the imperative of the principle are used for homogenous transition metal catalysis, photocatalytic and enzymatic reactions, polymer synthesis, solid processing operations that include crystallization reactions and aggregation flocculation, separation processes, liquid-liquid mixing, and extraction [71, 72].

It is significant to note that the angular velocity and gap size between the inner and outer cylinders affect the state of the flow of the liquid subjected to the Taylor-Couette principle/behaviour. R. Van Hout and J.Katz [73] reported this where they mentioned that as

the gap between the cylinders is reduced and the speed of the inner cylinder is increased, there is an increase in the instability of the flow as a result.

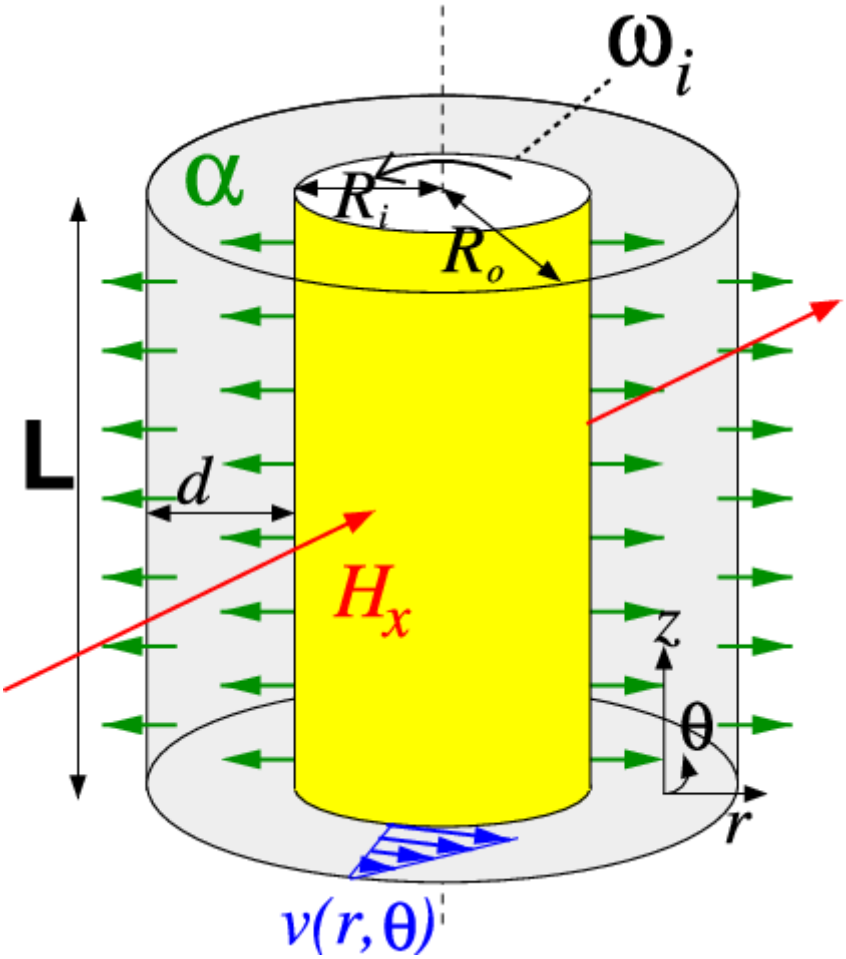


Figure 2.6: Schematic representation of the cylindrical Taylor Couette system [74]

Figure 2.6 provides a decent virtualization of the arrangement of the two cylinders in a reactor/set-up that applies the Taylor-Couette principle where the two cylinders are mounted on each other, with each cylinder having its own rotor. Thus, providing the freedom for each of the cylinders to rotate towards a direction that might be independent of that of the other cylinder.

With the Taylor-Couette flow, as the Reynolds number increases, the flow changes from being just circular Couette flow to being Taylor vortex flow, then to a state at which there are waves on the resulting vortices, then as the number furthers increases, the flow becomes turbulent

Taylor vortex flow [75]. In other words, at a low Reynolds number, which corresponds to low angular velocity, the flow is stable and steady as compared to higher Reynolds number (Corresponding to higher angular velocity) where the flow becomes chaotic and highly turbulent.

Before going any further, it is vital to highlight the concept of the Reynolds number and how it comes into action with regard to the Taylor-Couette flow.

Reynolds number is defined as the ratio of inertial forces to that of viscous forces of a fluid subjected to flow/movement, or the ratio of momentum convection and momentum diffusion length scales [76]. With the understanding of this definition, one can deduce the fact that at high Reynolds number, the flow would be unstable and turbulent, whereas, at a low Reynolds number, the flow would be gentle, and steady. Therefore, turbulent flow is associated with more inertial forces over viscous forces, whereas lamina flow is associated with forces that are more viscous over inertial forces.

Below is the formula to calculate the Reynolds number and the meaning of each parameter in the formula [75]:

$$Re = \frac{\mu . d}{v} \tag{3}$$

Where *Re* is the Reynolds number, μ is the rotation velocity of the inner cylinder, v is the kinematic velocity of the fluid, and d is the gap width (characteristic linear dimension).

Steady laminar flow occurs at Reynolds number in the range between 5 and 40, in this flow, there is an occurrence of a pair of symmetric counter-rotating vortices that form behind the cylinder. Based on the Reynolds numbers, there are laminar flow regimes that exist, namely the creeping laminar state where the flow is of Reynolds number in the range of 0 and 4, laminar flow with steady separation where the Reynolds number is in the range of 4 and 48, laminar

flow with periodic vortex shedding where the Reynold number is in the range of 48 and 180 [77].

When the flow is said to be laminar, it means that it is gentle, and the streamlines or rather the layers of the fluid flowing are parallel to each other. Whenever the Reynolds number is less than 2000, the flow is still considered a laminar flow [78]. During laminar flow, the fluid layers do not mix with each other, this is caused by the fluid particles moving with the same velocity where no layer of the fluid intersects with the adjacent layers.

Since it has been highlighted that laminar flow occurs at relatively lower Reynolds numbers, turbulent flow on the other side occurs at high Reynolds numbers where there is a mixing of fluid streamlines/layers, thus making the fluid flow unstable and chaotic.

2.6.3 Laminar flow reactor

A Laminar flow reactor is a micro-reactor that is used for continuous flow reactions. Compared to batch reactions where all the reagents are introduced to a reaction space all at the same time before the reaction occurs, reactions in the laminar flow reactor progress as the reagents are introduced into the reactor. Due to this, laminar flow reactors exhibit several advantages that make them favourable over conventional batch reactions.

There is a significant need to evaluate new, better, and more efficient synthetic routes in chemistry. This is due to the need for reduction of reaction costs, avoidance of loss of reagents/feeds and formation of unwanted products due to exposure to the external environment and minimizing time consumption so that there may be sufficient supply of the yields being produced.

A Laminar flow reactor as a continuous synthesis microreactor provides excellent heat transfer and enhanced mixing of reactants when compared to batch synthetic approaches. With these

reactors, there is high possibility of accurate reproducibility of reactions due to the excellent temperature control that the reactor has. With this microreactor, there is faster mixing of reagents via molecular diffusion, thus making it time efficient [79].

Batch reactions have become less preferred to several drawbacks such as heterogenous distribution of reactants, uneven temperature distribution, poor mixing of reagents, poor reproducibility of reactions due to poor control of the reaction conditions, difficulties in scaling up of reactions to produce larger yields, thus it leads to difficulties in shifting into commercial-scale production. With continuous reactors, there is also highly precise control of residence time, which leads to the yielding of narrow particle size distribution [80].

The excellent time efficiency of continuous reactors provides the opportunity to rapidly investigate physicochemical properties of the as-synthesized materials, thus leading to a faster and better understanding of new chemical materials, and a better understanding of material properties when reaction conditions are varied. Since the operating conditions can be easily and rapidly varied with precision, large databases can be created, which leads to a better understanding of the relationship between product properties, precursor properties and process conditions [81], this would also lead to better troubleshooting of reactions as a method to determine the best reaction conditions for production of the desired precursors and final products.

2.6.4 Microwave-assisted synthesis

Synthesis procedures and steps under which the as-prepared samples are subjected, significantly influence the material's physical and chemical properties. Since in this research, a sample that was prepared via the laminar approach was subjected to microwave irradiation, it is important to understand in brief detail the concept of microwave irradiation. This section highlights the principle of microwave irradiation and its benefits.

Microwave irradiation operates under electromagnetic radiation within the frequency region of 300 MHz to 300 GHz. The wavelengths associated with this energy are 1 mm to 1 m. With a larger frequency and shorter wavelength, large energy magnitudes result. During microwave irradiation, materials are subjected to dielectric heating. The materials absorb electromagnetic energy within their structures and convert that energy into heat energy. Due to the fact that the energy of a microwave photon at a frequency of 2.45 GHz is only $1.0x10^{-5}$ eV, that energy is not enough to break the chemical bonds of materials, thus it only affects molecular rotations [82].

This synthetic approach is a reliable option because when applied, there is a reduction of reaction times from hours to minutes as compared to conventional heating, hindrance of side reactions, thus sustaining the chemical integrity of the as-synthesized materials, increasing of yields and improvement of reproducibility [83]. These are some of the reasons why there has been many researchers applying microwave-assisted reactions for the optimization of chemical reactions.

Microwave processing of materials improves the quality of production and of as-synthesized materials, conserves human health from possible health issues posed by conventional methods of chemical material preparation, prohibits the excess hazards from being introduced to the environment and thus sustains the quality of human life [84].

Microwave irradiation is known for the fine-tuning of oxidation states of transition metal ions in cathode materials used in energy storage systems. When this method is applied to materials, there is an increase in the lattice parameters and unit cell volume, which has the potential to cause improved lithium-ion diffusion in the structure of materials. When materials are subjected to microwave irradiation, there is formation of oxygen vacancies due to entropy-driven desorption of oxygen from the lattice and charge balance in the lattice due to reduction

of oxidation states of transition metal ions. These modifications lead to improved specific capacity, capacity retention and rate capability. When materials are subjected to microwave irradiation, there is enhanced electronic conductivity, which ultimately leads to improved electrochemical performance [85].

This chapter focused on the significance of energy storage systems, supercapacitors, the constituents of supercapacitors, types of supercapacitors, theoretical modelling of supercapacitors, LMR-NMC cathode materials, the neeed to shift from LMR-NMC to MR-NMC with the advantages of this strategy discussed, and lastly, the synthetic approaches that were implemented in this project, with discussion on the advantages of these methods. Chapter 3, which is the one that follows, focuses on the methods of synthesis and the materials that were used for the synthesis of the metal oxide materials of focus.The chapter details the steps that were followed in the preparation of the materials.

Chapter 3

Methods and materials

3.1. Conventional and Laminar MR-NMC

3.1.1. Materials used

The materials used in this research project are listed below:

- $NiSO_4 \cdot 6H_2O$ (Sigma Aldrich)
- $CoSO_4 \cdot 7H_2O$ (Sigma Aldrich)
- $MnSO_4 \cdot H_2O$ (Sigma Aldrich)
- NH_4HCO_3 (Sigma Aldrich)
- Na_2CO_3 (Sigma Aldrich)
- PVDF (Sigma Aldrich)
- Carbon black Super C 45 (MSE supplies)
- rGO (Readily available in the lab, already synthesized before by postdoc using Hummers method)

The experimental approach followed in the conventional synthesis approach was obtained from a paper written by L.Li and colleagues [86] on NH_4F surface modificantion of Li-rich layered cathode materials.

The synthesis approach for the conventional approach is shown on **Figure 3.1**. In the synthesis of the samples, stoichiometric amounts of $NiSO_4 \cdot 6H_2O$, $CoSO_4 \cdot 7H_2O$, and $MnSO_4 \cdot H_2O$ (cationic ratio of Ni:Co: Mn = 0.13:0.13:0.54) were dissolved in deionised/distilled water to make a 2 mol L^{-1} aqueous solution of transition metal sulphates (MSO_4), the solution was

transferred into a three-neck flask. A mixed solution of 0.2 mol L^{-1} NH_4HCO_3 and 2 mol L^{-1} Na_2CO_3 (0.79 g of NH_4HCO_3 and 10.9 g of Na_2CO_3 were dissolved in 50 ml of distilled water) was slowly dripped into the magnetically stirred MSO_4 solution. The pH of the reaction was adjusted to 8.3, and the stirring speed was maintained at 1000 rpm under N_2 saturation. After further stirring for 24h, the conventionally coprecipitated $Ni_{0.13}Mn_{0.54}C_{0.13}(CO_3)$ precursor [Conv-NMC(CO_3)] was separated by centrifugation and washed several times with distilled water. To prepare the precursor using a laminar continuously stirred reactor (LCTR), MSO_4 solution and a mixed solution of NH_4HCO_3 and Na_2CO_3 were separately added into the reactor at controlled feeding rate of 20 ml min^{-1} through two peristaltic pumps, the controlled feeding rate was to ensure efficient mixing of the solutions. The pH of the reaction was also maintained to 8.3 using Na_2CO_3 which worked as both a precipitating and a pH controlling g agent, and the rotation speed was kept at 1000 rpm under N_2 saturation. After further stirring for 24 hr, the laminar coprecipitated $Ni_{0.13}M_{0.54}C_{0.13}(CO_3)$ [Lam-NMC(CO_3)] was obtained by centrifugation and washed several times with deionised water. The obtained transition metal carbonates [Conv-NMC(CO_3) and Lam-NMC(CO_3)] were then dried for 12 hr in air at 80 °C and mixed with Li_2CO_3 with 5% excess amount (1 g of MR-NMC was mixed with 0.7 g of Li_2CO_3), followed by calcining in air at 600 °C for 10 hr and then 800 °C for 16 hr in order to obtain Conventional-$LiNi_{0.2}Mn_{0.6}Co_{0.2}O_2$ (Conv MR-NMC) and Lam-$LiNi_{0.2}Mn_{0.6}Co_{0.2}O_2$ (Lam MR-NMC), respectively.

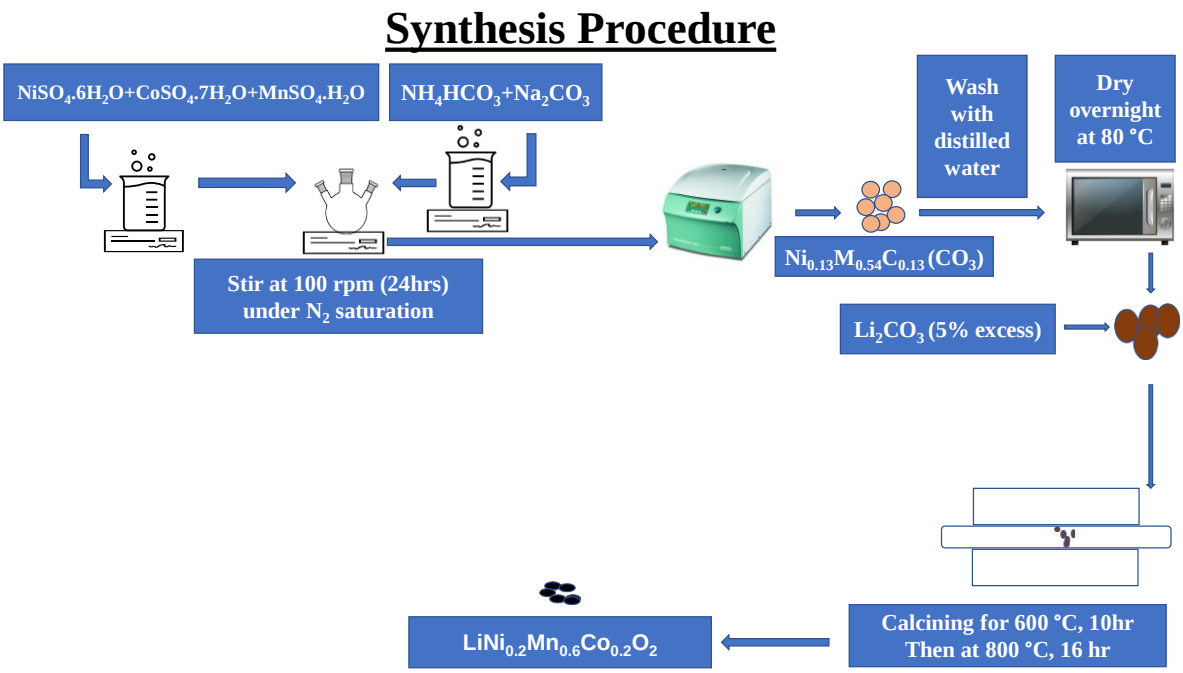


Figure 3.1: Schematic representation of the synthesis of MR-NMC (for laminar approach, the centrifuge is replaced with a laminar reactor)

To prepare the microwaved sample, 1.0 g calcined Lam MR-NMC was dissolved in 150 ml of ethylene glycol, 0.1 g of PVP was added, and the ratio of PVP to Lam MR-NMC was 1: 10. The mixture was stirred and then microwaved with a power of 600 W for 5 minutes (Using an in-house, custom built laboratorty microwave, 230 volts, 10 Amps minimum, 50 Hertz, single phase dedicated circuit). The product was washed with acetone and distilled water, then dried and annealed. The annealing conditions were the same as those of the conventional and the laminar samples. MW MR-NMC was obtained.

3.2 Material characterization

The morphology of the prepared samples were observed using TEM analysis which was performed on an FEI Tecnai T12 Spirit electron microscope operating at an accelerating voltage of 120 kV. For this analysis, the powdered samples were dispersed thanol, followed by

ultra-sonication for 3 minutes. The resulting suspension was then added dropwise on carbon-coated Cu grids before measurement was performed.

Structural features were analysed using X-ray diffraction (XRD) using a Bruker D2 phaser equipped with Cu-K_α radiation (λ=1.5405 Å) with an operating voltage of 30 kV and a current of 10 mA.

3.3 Electrochemical characterization

In the preparation of working electrodes for electrochemical studies of the materials, the active materials were crushed thoroughly and dispersed in ethanol and sonicated for 20 minutes to make a paste. The paste was evenly deposited on a circular carbon paper disk with an area of 1.131 cm^2 and dried at 80 °C in an oven overnight. For the three-electrode cells, the counter electrode used was a circular nickel foam disk of area 1.131 cm^2. Carbon paper was used as thereference electrode.

The SP300 Potentiostat (Bio-logic Science equipment operating on EC-Lab software) was used to perform cyclic voltammetry (CV), galvanostatic charge-discharge (GCD) and electrochemical impedance spectroscopy (EIS) 6M $LiNO_3$ aqueous electrolyte.

Chapter 4

Results and discussion

The use of electrical energy storage (EES) methods is crucial for the rapid advancement of electric vehicles, portable devices, and grid storage systems [87]. Lithium-ion batteries (LIBs) are a popular choice among various electrochemical EES systems for energy storage and delivery, as they offer high energy densities of up to ~300 Wh kg^{-1} and a reasonable cycling life of about 2000 cycles. However, LIBs have limited power densities (below 1 kW/kg) [88]. On the other hand, electrical double-layer capacitors, also known as supercapacitors, have the ability to quickly transport charges due to their impressive power density (<15 kW/kg). Therefore, it is important to develop EES devices that have high energy densities of at least tens of Watt-hours per kilogram and can provide power densities and durability that are similar to supercapacitors. This is especially crucial because of the urgent demand for energy storage devices for intermittent systems, like solar panels and wind turbines. Recently, hybrid supercapacitors have been under investigation as new energy storage devices that combine the benefits of supercapacitors and LIBs [89]. This is due to the fact that they can offer long cycle life, high energy density, and power density. These hybrid supercapacitors are generally made up of a mixed system that includes a transition-metal oxide anode resembling a battery and an activated carbon (AC) cathode resembling a capacitor [90]. Hybrid supercapacitors store electric charge through a dual process that involves both physical adsorption/desorption of anions and chemical Li-ion intercalation/deintercalation. Hybrid supercapacitors can deliver much more energy than supercapacitors without sacrificing the power density using new electrode materials that increase the operating voltage window [91].

LMR-NMC cathode material has significantly gained more attention for application in lithium-ion batteries due to their high capacity which surpasses 250 $mAhg^{-1}$. The material has Li_2MnO_3 and Li_2MnO_3-like counterparts that are with a short-range order within a $LiMO_2$ matrix. However, this material suffers from large capacity fade that is irreversible in the first cycle depending on their composition. This capacity loss is attributed to the extraction of two lithium ions from Li_2MnO_3 during charging and the failure to insert all the lithium ions back into the lattice during discharging [92].

There is a need to inhibit the challenges that are associated with LMR-NMC that have also been highlighted in the previous chapters. One of the strategies to resolve those drawbacks and improve the overall performance of these materials is exploring the chemistry of the materials by varying the ratios of the transition metal ions that compose them. Chemical composition of lithiated transition metal oxides has a significant influence on the operation of LMR-NMC cathode materials [93].

The results that follow focus on MR-NMC cathode material applied in hybrid supercapacitor as the cathode material, whereas rGO is applied as a anode material. The metal oxide uses faradaic charge storage mechanism, the rGO uses non-faradaic charge storage mechanism. This is implemented to improve both the energy and power density of the system, thus bridging the gap between batteries and capacitors.

4.1 Physicochemical characterization

Power X-ray diffraction (XRD) patterns of conventional, laminar and microwaved samples were obtained for the evaluation of the materials' crystallinity as shown on **Figure 4.1**:

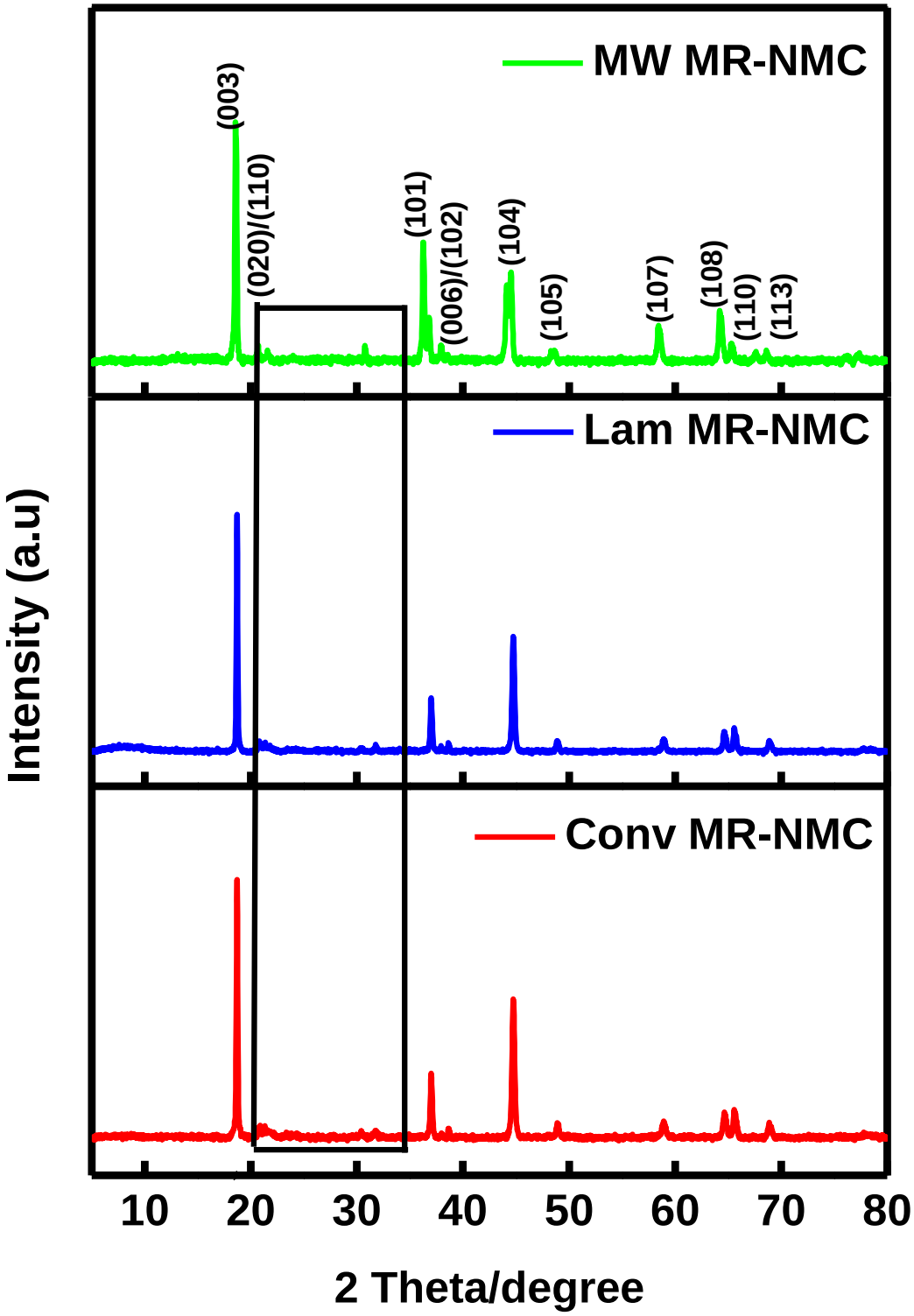


Figure 4.1: XRD patterns of the as-synthesized samples

From the XRD patterns obtained, the peaks at the indices (003), (101), (006), (102), (104), (105), (107), (108), (110) and (113) can be attributed to the $LiMO_2$ phase of the materials, which are a result of the presence of the hexagonal structure that belongs to the *R*3m space group, with a PDF number of 00-056-0147. The minor and less intense peaks that are within the 20-35 º (Grouped in the box shown on the figure) range correspond to the Li_2MnO_3 phase that result from the monoclinic phase of the *C2/m* space group [85]. The XRD patterns confirm the presence of two phases that were expected during synthesis. Fortunately, there was no sign of any foreign or unexpected peaks on the patterns of the samples, which is a significant indicator of the absence of any possible impurities in the samples.

The presence of narrow peaks on the patterns for the samples indicates high crystallinity of the as-synthesized materials. For the three materials, the $I_{(003)}/I_{(104)}$ ratios were calculated using the intensities of the peaks of the respective miller indices, these values are an indicator of the extent of cation mixing. Cation mixing compromises the structural integrity of the materials and therefore deteriorates the electrochemical performance of the materials [94]. When the values are greater than 1.2, there is negligible cation mixing. The obtained values for the conventional, laminar, and microwaved materials were 1.86, 2.06 and 2.75, respectively. This means that there was negligible cation mixing for the three samples, but more negligible for the microwaved sample, thus emphasizing the structural integrity of the microwaved material being the best amongst the three materials, which leads to enhanced cycle performance and stability. The lower degree of cation mixing in the microwaved material can be attributed to the subjection of the material to microwave irradiation.

Looking at the stacked XRD patterns on **Figure 4.1**, the peaks of the microwaved material had a shift towards lower 2 θ angles as compared to the XRD patterns of the conventional and laminar materials that are superimposed. It has been reported that a shift towards lower 2 θ on XRD patterns is an indicator of lattice expansion, this is potentially the case with the

microwaved material studied in this project [95]. Lattice expansion provides wider channels for the movement of ions, thus improving the electrochemical performance of the material, which is a phenomenon that is associated with microwave irradiation.

TEM images for the conventional and laminar samples were obtained to evaluate the morphology of the materials as shown on **Figure 4.2**:

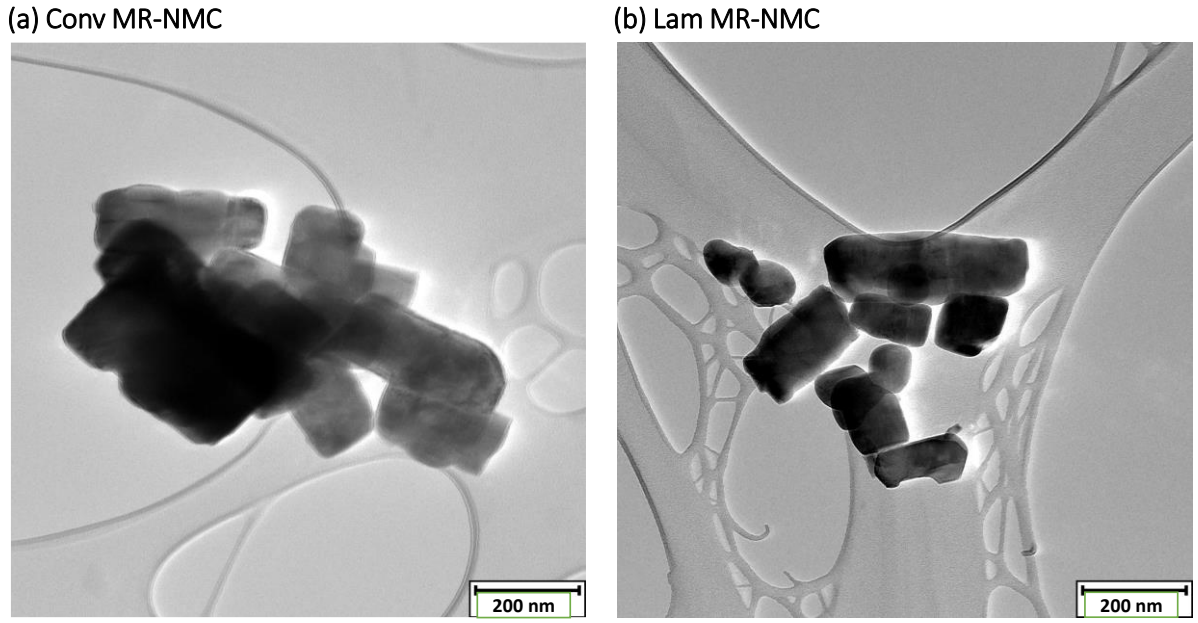


Figure 4.2: TEM images of (a) Conv MR-NMC and (b) Lam MR-NMC.

As evident in the **Figure 4.2**, there seems to be agglomeration on both samples, this has the potential to decrease the active surface area of the nanoparticles, thus reducing their electrochemical performances. Agglomeration can also block the available pores of the nanoparticles, which would hinder access of the material surface by the electrolyte. Another cause of the observed morphology could be the sample preparation for TEM analysis, which could have affected the observed images. Better TEM analysis/HRTEM might provide clear characterization to draw solid conclusive remarks about the material's morphology. The images demonstrate irregular and spherical morphology of the materials (Mixed

morphologies). On the TEM images, the particles are big and defined, this corroborate with the high intensity peaks on the XRD which suggests high crystallinity.

4.2 Electrochemical characterization

The synthesis process of MR-NMC is illustrated in **Figure 3.1**. All MR-NMC materials were mixed with the conductive carbon black (Super C45) and poloyvinylidene fluoride (PVDF) binder (at a weight ratio of 70 : 20 : 10), and then N-methyl pyrrolidinone (NMP) solvent was added. The resulting slurry were applied onto carbon paper through drop casting and the electrodes were then dried at 80°C overnight to evaporate the NMP solvent. The rGO electrode was prepared in the same manner, except carbon black was not included.

Figure 4.3(a) shows a schematic of a hybrid supercapacitor fabricated using MR-NMC as the positive electrode and rGO as the negative electrode in 6 M $LiNO_3$ aqueous electrolyte. Before fabricating the hybrid supercapacitors, the performance of the individual electrodes (MR-NMC and rGO) was screened through a three-electrode system (half-cell tests), as shown in **Figure 4.3b(i-ii)**. The CV curves of MR-NMC were plotted in the potential range of 0.5 to 1.4 V at a scan rate of 10 mV/s, while the rGO was plotted in the potential range of 0.0 to -0.8 V at a scan of 10 mV/s. Only the MW-MR-NMC CV is presented because it performed better than the other two cells during cycling, thus it is selected for demonstration of the metal oxide materials being combined with the rGO for the assembly of the hybrid cells. The CV curve of rGO in 6 M $LiNO_3$ electrolyte, as shown in **Figure 4.3b(i)**, appears nearly rectangular, indicating exceptional electrical double-layer capacitive behaviour [96]. In contrast, the CV curve of MR-NMC, as seen in **Figure 4.3b(ii)**, shows pseudocapacitive behaviour with redox peaks around 1.1 and 0.7 V corresponding to the intercalation/deintercalation of Li-ions in the layered MR-NMC structure. The CV patterns with peaks are as a result of redox reactions which are attributed to pseudocapacitance [97]. For the fabrication of a full cell (rGO//MR-NMC), a ratio of 1:3 was maintained for all the cells. **Figure 4.3b(iii)** shows the CV curves of rGO//MW MR-NMC at different cell potentials. The CV curves exhibit both an electric double layer (i.e., <

1.0 V) and pseudocapacitive nature at high potentials (i.e., > 1.0 V). This shows a good synergy between rGO and MW MR-NMC electrode material.

Figure 4.3c shows the CV curves of three hybrid capacitors at a cell potential range of 0.0 V to 1.7 V. The advantage of combining a capacitive and a battery material was the improvement of the overall potential of the cells, which contributes to the enhancement of the capacitance of energy storage systems. The CV curves of rGO//Conv MR-NMC and rGO//Lam MR-NMC are nearly rectangular with no prominent redox peaks, indicating that the energy storage mechanism is dominated by a surface-controlled electric double-layer capacitance (EDLC) and at a 1:3 ratio, rGO serves as the capacity limiting electrode. In contrast, the CV curve of rGO//MW MR-NMC shows both EDLC and pseudocapacitive storage mechanisms with visible redox peaks at higher cell potentials. Additionally, the rGO//MW MR-NMC cell has a higher current response than the other two cells, indicating a higher capacitance. Galvanostatic charge/discharge (GCD) was also used to compare the three hybrid capacitors, and it was observed that the rGO//MW MR-NMC cell exhibits redox plateaus and a longer discharge time than the other two hybrid capacitors. The GCD for the rGO//Conv MR-NMC and rGO//Lam MR-NMC cells shows nearly symmetrical triangle charge/discharge profiles, indicating exceptional EDLC behaviour [98]. The specific capacitance of the three hybrid capacitors was calculated using the GCD (see equation 4 [99]). At the current density of 0.2 A g^{-1}, rGO//MW MR-NMC, rGO//Lam MR-NMC and rGO//Conv MR-NMC had a specific capacitance of 44.77 F g^{-1}, 15.89 F g^{-1} and 13.68 F g^{-1}, respectively. rGO//MW MR-NMC performed better than the other two cells in terms of specific capacitance. The results indicate that the rGO//MW MR-NMC hybrid capacitors have the highest discharge capacitance compared to the other two cells, consistent with the CV and GCD data. The specific capacitance decreases as the current density increases, as at high current density, the electrolyte ions cannot penetrate the bulk of the electrode material. The high specific capacitance of the rGO//MW-MR-NMC cell can

attributed to the microwaved assisted synthesis, the approach potentially introduced lattice expansion of the metal oxide material as mentioned previously, which could have improved the movement of ions in and out of thr material asa compared to the other materials.

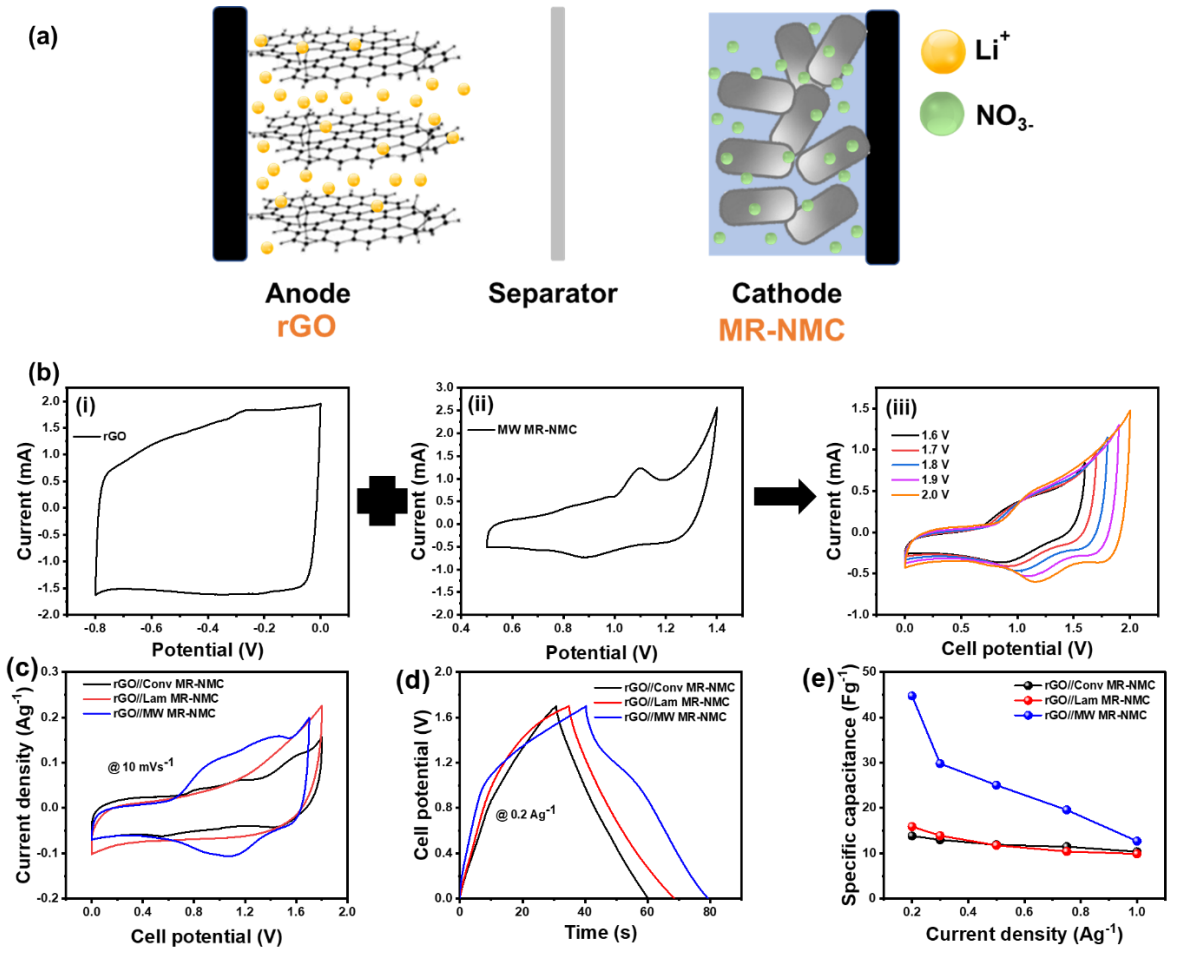


Figure 4.3: (a) Schematic representation of a hybrid supercapacitor made of rGO and MR-NMC, (b) CV of (i) rGO and (ii) MR-NMC combined to form overall CV of the hybrid supercapacitor, (iii) CV of hybrid rGO//MR-NMC from the combination of rGO and MR-NMC (c) CV plots of rGO//Conv MR-NMC, rGO//Lam MR-NMC and rGO//MW MR-NMC, (d) GCD of rGO//Conv MR-NMC, rGO//Lam MR-NMC and rGO//MW MR-NMC, (e) Current density vs specific capacitance of rGO//Conv MR-NMC, rGO//Lam MR-NMC and rGO//MW MR-NMC

The equations that follow were used to calculate the specific capacitance values, maximum specific power density and specific energy density of the assembled cells [99] :

$$C_{sp} = \frac{4.C}{m} \quad (4)$$

$$P_{max}(10^3 W/kg) = \frac{V2}{4mRs} \quad (5)$$

$$E(\frac{1}{3.6} wh/kg) = \frac{CV2}{2m} \quad (6)$$

Where *C*(F) is the capacitance, m is the total mass of the two electrodes, *V*(V) is the maximum voltage acquired during charge, R_s is the equivalent series resistance obtained from the *IR* drop on GCD .

$$Rs = \frac{\Delta VIR}{2i} \quad (7)$$

Where ΔV_{IR} is the voltage drop between the first two points from the start of the discharge curve, and *i*(A) is the applied current.

Electrochemical impedance spectroscopy (EIS) can be useful for determining the electrochemical properties of various materials. **Figure 4.4** illustrates the EIS measurements of three hybrid capacitors, and a Nyquist plot is modelled using a combined RC/Randles circuit. This circuit includes different components, such as resistance due to the solid electrolyte interface (SEI), charge-transfer resistance (R_{ct}) due to electron transport, interfacial resistance (R_{int}) due to IR drop, double-layer capacitance (C_{dl}), and constant phase elements (CPE_{ct} and CPE_{cs}). The equivalent circuit shown in **Figure 4.4a** was utilized to fit the EIS data, and the impedance of the constant phase element (Z_{CPE}) follows a power-law relationship described by equation 8 [100].

$$Z_{CPE} = [Q\ (j\omega)^a]^{-1} \quad (8)$$

The exponent "a" in the equation represents the slope of the log *Z* vs. log *F*, which ranges from -1 to 1. A CPE with a = 0 is a pure resistor, while a = 1 represents a pure capacitor, and a = -1 indicates an inductor. A CPE with a = 0.5 is equivalent to the Warburg impedance (Z_w) [94]. The Nyquist plot for rGO//MW MR-NMC has a larger semicircle diameter, suggesting greater Faradaic reactions at the active surface of the hybrid supercapacitor, this is due to the fact that the diameter of the semicircle at lower frequencies and the conductivity of the electrode exhibit direct proportionality [101]. In contrast, the semicircles of rGO//Conv MR-NMC and rGO//Lam MR-NMC hybrid capacitors are smaller, indicating low charge transfer resistance.

Table 4.1 shows the series resistance values ($R_s + R_{sei} + R_{ct} + R_{int}$) of three different hybrid supercapacitors: rGO//Conv MR-NMC, rGO//Lam MR-NMC, and rGO//MW MR-NMC. The values for each are 110.83, 216.17, and 93.14 Ω, respectively. These results demonstrate that the rGO//MW MR-NMC hybrid supercapacitor has the lowest series resistance and therefore better conductivity. The rGO//Conv MR-NMC and rGO//Lam MR-NMC capacitors show a more vertical line in the low-frequency region, indicating strong capacitive behaviour [102]. In the high-frequency region, the charge transfer resistance at the electrode/electrolyte interface is reflected by the diameter of the quasi-semicircle. **Table 4.1** shows that the Rct value of rGO//Conv MR-NMC (3.66 Ω) is smaller than that of rGO//Lam MR-NMC (5.69 Ω) and rGO//MW MR-NMC (7.37 Ω). This could be because of the high capacitive contribution of rGO in the hybrid cell [103].

Table 4.1: EIS results of rGO//Conv MR-NMC, rGO//Lam MR-NMC and rGO//MW MR-NMC hybrid supercapacitors

Hybrid cells	rGO//Conv MR-NMC	rGO//Lam MR-NMC	rGO//MW MR-NMC
R_s (Ω)	0.62 ± 0.06	0.52 ± 0.21	0.49 ± 0.05
R_{sei} (Ω)	2.35 ± 0.43	14.54 ± 9.45	12.68 ± 0.04
R_{ct} (Ω)	3.66 ± 0.22	5.69 ± 0.94	7.37 ± 6.35
R_{int} (Ω)	104.2 ± 10.14	195.42 ± 7.99	72.58 ± 12.27
C_{dl} (mF)	19.71 ± 0.16	35.11 ± 3.80	11.58 ± 4.80
CPE_{ct} (mF. s^(a-1))	0.52 ± 0.26	0.10 ± 0.06	0.20 ± 0.05
CPE_{cs} (mF. s^(a-1))	11.66 ± 0.25	87.13 ± 2.25	7.69 ± 0.96
a	0.8	0.8	0.6

The approximation of the rGO//MR NMC interface as a simple circuit consisting of a resistor and a capacitor in series was used to estimate the real part of capacitance (C′) across the frequency range (10 mHz to 10 Hz) in the capacitive regime of frequencies [104]. The impedance analysis of the hybrid supercapacitors was used to determine the values of C′, which is shown in **Figure 4.4c**. The real part of capacitance (C′) and imaginary part of capacitance (C″) were calculated using the following equations [105]:

$$C' = \frac{-Z''}{2\pi f |Z|^2} \tag{9}$$

$$C'' = \frac{Z'}{2\pi f |Z|^2} \tag{10}$$

where |Z| is the absolute value of impedance (Ω), while Z′ and Z″ are the real and imaginary components of impedance, respectively, and f is the frequency (Hz).

The phase angle can be calculated using the following equation [106]:

$$\emptyset = -\tan^{-1} \frac{Z' \omega}{Z'' \omega} \quad (11)$$

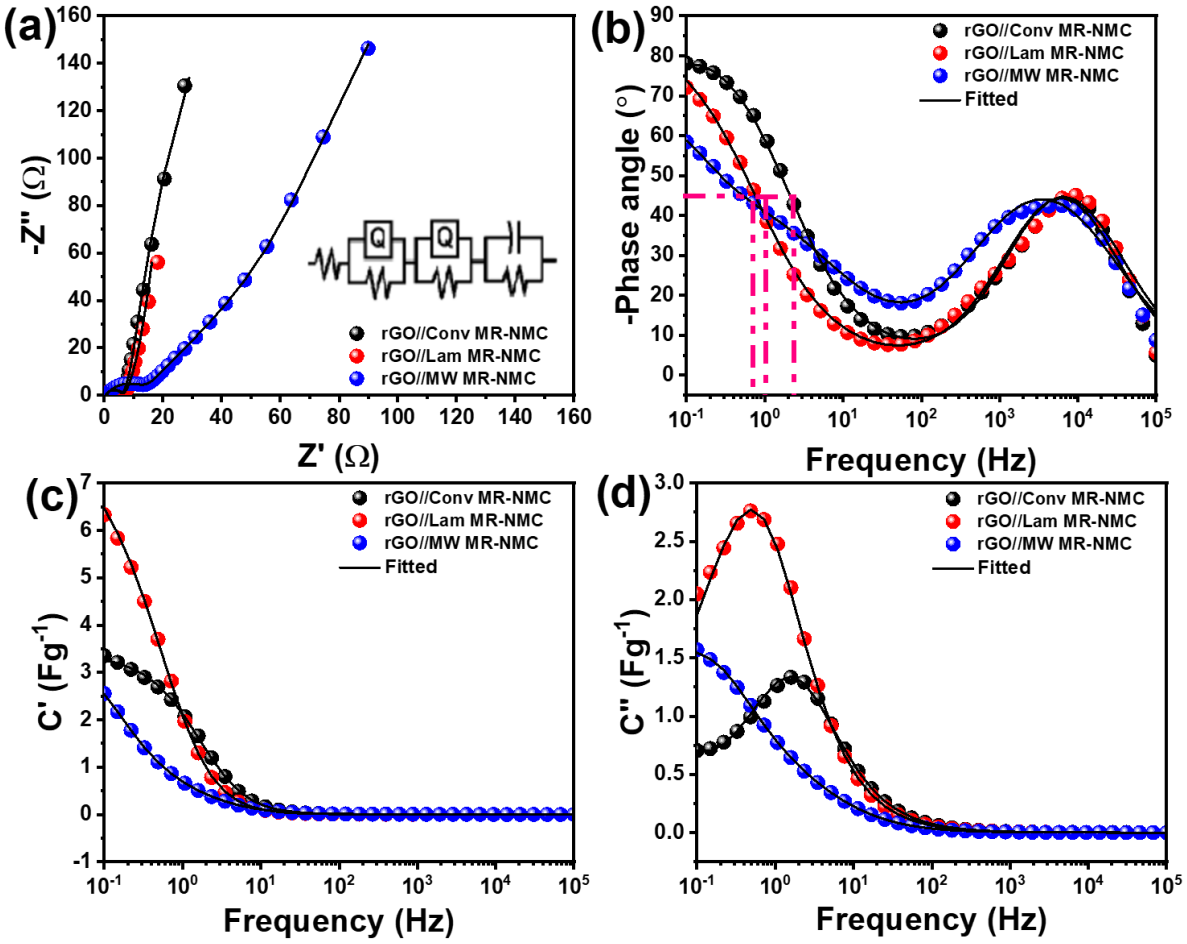


Figure 4.4: (a) Nyquist plots of rGO//Conv MR-NMC, rGO//Lam MR-NMC and rGO//MW MR-NMC hybrid supercapacitors (insert, electrical circuit used to fit the impedance data), (b) Bode plot of rGO//Conv MR-NMC, rGO//Lam MR-NMC and rGO//MW MR-NMC hybrid supercapacitors, (c) real capacitance, C′ and (d) imaginary capacitance, C″ with frequency for rGO//Conv MR-NMC, rGO//Lam MR-NMC and rGO//MW MR-NMC hybrid supercapacitors

The rate of charge storage kinetics can be determined by analysing the relationship between phase angle (*Ø*) and frequency (*f*), as shown in **Figure 4.4b**. The phase angle can be calculated using the equation 11 [106]. A phase angle of 0° indicates pure resistance, while -90° indicates capacitive behaviour, and -45° indicates a diffusion-limited response [107], where the

impedance of a hybrid capacitor is equal to the resistance of a resistor in an equivalent series resistor-capacitor model. To understand the responses in different hybrid supercapacitors, 2D Bode plots of $\emptyset$ vs. f are shown in **Figure 4.4b**. For the rGO//Conv MR-NMC hybrid supercapacitor, the phase angle is -78° at a low frequency of 10 mHz, compared to -72° for rGO//Lam MR-NMC and -58° for rGO//MW MR-NMC cells. This difference is due to the more prominent redox processes at low frequencies in the rGO//MW MR-NMC hybrid cell compared to the other two hybrid capacitors [108]. A phase angle of -45° is considered the transition point between capacitive and resistive behaviour, indicated by a horizontal dotted line in **Figure 4.4b**. The cross-over frequency in rGO//Conv MR-NMC hybrid supercapacitor is 2.4 Hz, meaning resistance dominates for charging times less than 0.42 seconds. For the rGO//Lam MR-NMC and rGO//MW MR-NMC hybrid cells, the cross-over frequency is 0.68 Hz, indicating resistance dominates for a charging time less than 1.47 seconds.

Figure 4.4c shows a graph that represents the frequency-dependent behaviour of the real capacitance (C′) for three different hybrid capacitors. The capacitance values of all three hybrid capacitors decrease with an increase in frequency up to 100 Hz, and then they remain constant. Among the three hybrid cells, the rGO//Lam MR-NMC shows the highest capacitance, followed by rGO//Conv MR-NMC and rGO//MW MR-NMC hybrid capacitor. It is important to note that at higher frequencies, the capacitance decreases as the penetration of electrolyte ions is limited by the outer surface of the electrode, and the inner surface is not accessible. To quantify the frequency response, the imaginary capacitance, C″ vs. frequency, *f*, was derived from the EIS data, and the resulting convex curves' maxima represent the frequency (f_0) at which purely resistive behaviour transitions into purely capacitive behaviour (see **Figure 4.4d**). The relaxation time constant (τ_0), which measures how quickly the device can be charged and discharged, is calculated as the reciprocal of f_0 using the equation: $\tau_0 = 1/2\pi f_0$ [105]. The calculated τ_0 values for the rGO//Conv MR-NMC and rGO//Lam MR-NMC hybrid capacitors

are 0.59 s and 2 s, respectively. A lower τ_0 value is preferable for electrochemical capacitor devices to ensure fast charge-discharge characteristics [105]. Therefore, the low τ_0 for the rGO//Conv MR-NMC suggests faster access to electrolyte ions during the electrochemical process.

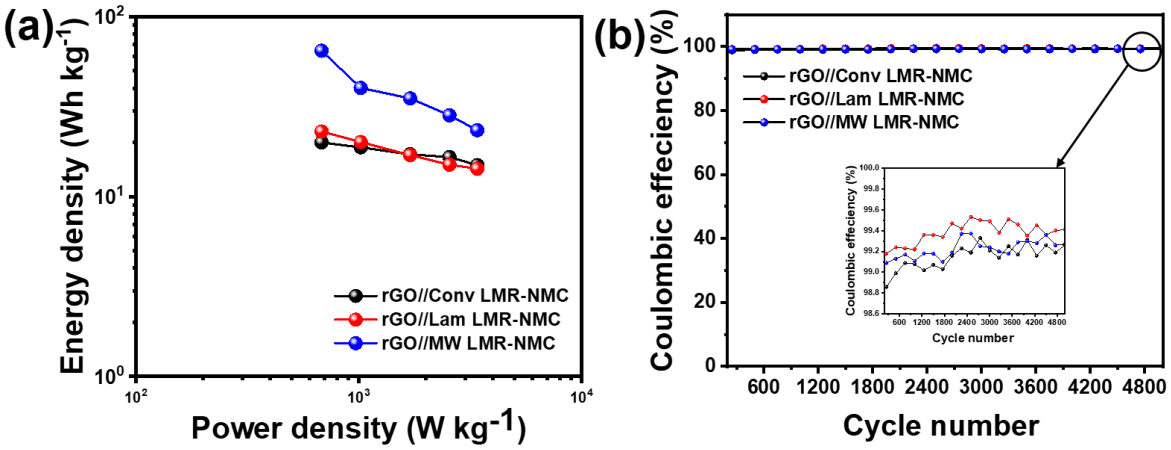


Figure 4.5: (a) Power density vs energy density of the three assembled full cells, (b) Coulombic efficiency of the three assembled full cells

As it can be seen on **Figure 4.5a**, rGO//MW MR-NMC had the best energy density response over the entire range of power density. There is no significant difference in the energy density responses of the other two cells over the entire power density range. At the power density of 678.08 W kg^{-1}, rGO//MW MR-NMC, rGO//Lam MR-NMC and rGO//Conv MR-NMC had a maximum energy density of 65.05 Wh kg^{-1}, 23.45 Wh kg^{-1} and 19.82 Wh kg^{-1}, respectively. rGO//MW MR-NMC out-performed the other two cells in terms of maximum energy density by a significant margin. The high energy density over the entire range of power density for the rGO//MW-MR-NMC was potentially caused by the lattice expansion phenomenon caused by the microwaved assisted synthesis approach mentioned previously.

Figure 4.5b exhibits good coulombic efficiency for the three full cells over 5000 cycles. Coulombic efficiency is the ratio of the time it takes to discharge a cell to the time it takes to charge the cell. A coulombic efficiency that is ~100% is an indicator of an excellent balance between charging and discharging times. In other words, the time it takes to charge the cell is precisely close to the time it takes to discharge the cell, this is important because we would not need a cell that charges longer and then discharges quicker, such system would not be energy efficient. This also shows that the system has excellent elechtrochemical stability. The three full cells had desirable coulombic efficiency. Therefore, these systems had the ability to discharge a high amount of charge that was originally stored with no significant unwanted losses, which makes them an interest in energy storage systems.

Table 4.2: Comparison of maximum energy densities of other asymmetric hybrid supercapacitors and asymmetric supercapacitors studied in this work

Full cell	**Electrolyte**	**Voltage(V)**	**Energy density$_{max}$ (Wh kg^{-1})**	**References**
$K_{0.45}MnO_2.0.3H_2O$//AC	Aqueous K_2SO_4	0-1.65	43.10	[109]
AC//Bi_2O_3@C	Aqueous Na_2SO_4-NaCl	0-1.9	18.94	[110]
ZnNiCo-P//rGO	Aqueous KOH	0-1,6	60.10	[111]
$KNiPO_4$//AC	Aqueous KOH	0-1.5	13.40	[112]
Co_2S_4@N-doped CNT//AC	Aqueous KOH	0-0,5	49.75	[113]
3D CoO@PPy//AC	Aqueous KOH	0-1.8	43.50	[114]
(Cu, Ni)O//AC	Aqueous KOH	0-1.8	50.3	[115]
rGO//Conv MR-NMC	Aqueous $LiNO_3$	0-1.7	19.82	This work

rGO//Lam MR-NMC	Aqueous $LiNO_3$	0-1.7	23.45	This work
rGO//MW MR-NMC	Aqueous $LiNO_3$	0-1.7	65.05	This work

As evident on **Table 4.2**, rGO//MW MR-NMC cell outperformed some of the asymmetric hybrid supercapacitors that have been studied in terms of maximum energy density. This emphasizes that this system has the potential to mitigate energy crisis. If further research is conducted on this supercapacitor together with subjecting MR-NMC under laminar synthetic approach and microwave irradiation, it is promising that the hybrid supercapacitor can be commercialized and bridge the gap between energy demand and supply.

Chapter 5

Conclusion and recommendations

In this study, manganese-rich NMC materials were synthesized via a conventional method (co-precipitation), a laminar method and microwave irradiation. The materials were used with reduced graphene oxide to assemble a two-electrode asymmetric hybrid supercapacitor. Three hybrid cells were therefore studied, and their performances were compared amongst each other.

Physical characterization was performed for the MR-NMC samples using TEM and XRD. XRD was performed to evaluate the crystalline nature and the crystal phases present in the samples. The XRD patterns obtained for the as-synthesized samples matched with the ones reported in the literature for the same nature of material, with the peaks for the MW MR-NMC having shifted to low 2 theta angles, which indicates lattice expansion that is beneficial for diffusion kinetics. TEM was performed for evaluation of the morphology of the samples, where one-dimensional rod morphology was evident with presence of agglomeration.

Electrochemical performances of the three-electrode (Half-cell) and two-electrode (Full cell) systems were evaluated using cyclic voltammetry and galvanostatic charge-discharge. The specific capacitance of the three full cells were calculated.. At the current density of 0.2 A g^{-1}, rGO//MW MR-NMC, rGO//Lam MR-NMC and rGO//Conv MR-NMC had specific capacitance of 44.77 F g^{-1}, 15.89 F g^{-1} and 13.68 F g^{-1}, respectively. Making rGO//MW MR-NMC cell the best performing amongst the three. Specific energy and power density of the three full cells assembled were calculated. At the power density of 678.08 Wh kg^{-1}, rGO//MW MR-NMC had the highest specific energy density of 65.05 Wh Kg^{-1}, followed by rGO//Lam MR-NMC which had 23.45 Wh kg^{-1}, then rGO//Conv MR-NMC with 19.82 Wh kg^{-1}, making rGO//MW MR-NMC the best performing cell amongst the three cells studied. Amongst these cells, the rGO//MW MR NMC performed the best in terms of specific energy and power

density. rGO//MW MR-NMC also surpassed some reseasrched asymmetric supercapacitors in aqueous electrolytes, which potentially makes the system one of the hybrid supercapacitors of interest for energy storage.

In conclusion, this work has proven that the use of laminar flow approach and microwave irradiation together improve the electrochemical performance of MR-NMC and make it competitive against other transition metal based materials used in energy storage, which makes the material an excellent candidate to be applied in asymmetric hybrid supercapacitors.

Future work

There are several implementations that can be considered in the attempt to improve the performance of the cells studied in this work.

In the electrochemical studies phase, cycling should be performed for longer cycles at lower scan rates and current densities to give the materials enough time to activate fully. Cell assembly should be done carefully to avoid any possible human error, or rather use a cell that would not compromise the material structural integrity during assembly, and one that is not susceptible to excessive electrolyte leakage and drying. This would also ensure that there is no electrolyte refilling during cycling, which would be at times inconsistent amongst the cells studied since some electrochemistry might show signs of the need for a refill, while others might not.

Another possibility of poor electrochemical behaviour of materials might be dissolution when the structural integrity is compromised during cycling, to avoid this, coating and doping can be a better approach, especially coating or doping with materials that are conductive to also

improve on the conductivity of the materials further. In future work, coating can be performed using CeO_2 due to the benefits that the metal oxide possesses.

Focus can also be shifted towards the electrolyte used to improve performance. Organic or hybrid(organic-aqueous) electrolytes should be applied to have the ability of using high working potential window to improve capacitance responses, specific energy, and power density. The use of higher potential windows might also lead to the activation of the material's additional monoclinic phase that leads to an increase in capacitance. Other aqueous electrolytes can also be explored with electrolyte additives for application in hybrid supercapacitors. Other metal oxides can also be studied for application with reduced graphene oxide in asymmetric hybrid supercapacitors.

More work should be the characterization of the materials with more techniques to get the rich understanding of the samples used in this research, this includes SEM, BET and XPS. There has also not been TEM characterization of the microwaved material, this should be conducted in the future as well to have an insight of the material's morphology when compared to the other two.

REFERENCES

[1] Panwar, N. L., Kaushik, S. C., & Kothari, S. (2011). Role of renewable energy sources in environmental protection: A review. *Renewable and Sustainable Energy Reviews*, *15*, 1513–1524.

[2] Nicoletti, G., Arcuri, N., Nicoletti, G., & Bruno, R. (2015). A technical and environmental comparison between hydrogen and some fossil fuels. *Energy Conversion and Management*, *89*, 205–213.

[3] Iodice, P., Dentice D'Accadia, M., Abagnale, C., & Cardone, M. (2016). Energy, economic and environmental performance appraisal of a trigeneration power plant for a new district: Advantages of using a renewable fuel. *Applied Thermal Engineering*, *95*, 330–338.

[4] Hoel, M., Kverndokk, S. (1996). Depletion of fossil fuels and the impacts of global warming. *Resource and Energy Economics* , *18*, 115-136.

[5] Machol, B., & Rizk, S. (2013). Economic value of U.S. fossil fuel electricity health impacts. *Environment International*, *52*, 75–80.

[6] Mohtasham, J. (2015). Review Article-Renewable Energies. *Energy Procedia*, *74*, 1289–1297.

[7] Solarin, S. A., Bello, M. O., & Bekun, F. V. (2021). Sustainable electricity generation: the possibility of substituting fossil fuels for hydropower and solar energy in Italy. *International Journal of Sustainable Development and World Ecology*, *28*, 429-439.

[8] Bose, B. K. (2010). Global warming: Energy, environmental pollution, and the impact of power electronics. *IEEE Industrial Electronics Magazine*, *4*, 6–17.

[9] Freedman, B. (2014). Population growth and global change. *Global Environmental Change*, *18*, 571–577.

[10] Vrrousek, P. (1994). Beyond Global Warming: Ecology and Global Change. *Ecology*, *75*, 1861–1876.

[11] Nordell, B. (2003). Thermal pollution causes global warming. *Global and Planetary Change*, *38*, 305–312.

[12] Barbir, F., Veziroğlu, T. N., & Plass, H. J. (1990). Environmental damage due to fossil fuels use. *International Journal of Hydrogen Energy*, *15*, 739–749.

[13] Amirante, R., Cassone, E., Distaso, E., & Tamburrano, P. (2017). Overview on recent developments in energy storage: Mechanical, electrochemical and hydrogen technologies. *Energy Conversion and Management*, *132*, 372–387.

[14] Moriarty, P., & Honnery, D. (2016). Can renewable energy power the future? *Energy Policy*, *93*, 3–7.

[15] Gielen, D., Boshell, F., Saygin, D., Bazilian, M. D., Wagner, N., & Gorini, R. (2019). The role of renewable energy in the global energy transformation. *Energy Strategy Reviews*, *24*, 38–50.

[16] Mitali, J., Dhinakaran, S., & Mohamad, A. A. (2022). Energy storage systems: a review. *Energy Storage and Saving*, *1*, 166–216.

[17] Olabi, A. G., & Abdelkareem, M. A. (2021). Energy storage systems towards 2050. *Energy*, *219*, 119634.

[18] Lukic, S. M., Cao, J., Bansal, R. C., Rodriguez, F., & Emadi, A. (2008). Energy storage systems for automotive applications. *IEEE Transactions on Industrial Electronics*, *55*, 2258–2267.

[19] Thackeray, M. M., Wolverton, C., & Isaacs, E. D. (2012). Electrical energy storage for transportation - Approaching the limits of, and going beyond, lithium-ion batteries. *Energy and Environmental Science*, *5*, 7854–7863.

[20] Wang, F., Wu, X., Yuan, X., Liu, Z., Zhang, Y., Fu, L., Zhu, Y., Zhou, Q., Wu, Y., & Huang, W. (2017). Latest advances in supercapacitors: From new electrode materials to novel device designs. *Chemical Society Reviews*, *46*, 6816–6854.

[21] Masaud, T. M., Lee, K., & Sen, P. K. (2010). An overview of enrgy storage technologies in electric power systems: What is the future? *North American Power Symposium 2010,* 1-6.

[22] Libich, J., Máca, J., Vondrák, J., Čech, O., & Sedlaříková, M. (2018). Supercapacitors: Properties and applications. *Journal of Energy Storage*, *17*, 224–227.

[23] Jiao, Y., Pei, J., Chen, D., Yan, C., Hu, Y., Zhang, Q., & Chen, G. (2017). Mixed-metallic MOF based electrode materials for high performance hybrid supercapacitors. *Journal of Materials Chemistry A*, *5*, 1094–1102.

[24] Muzaffar, A., Ahamed, M. B., Deshmukh, K., & Thirumalai, J. (2019). A review on recent advances in hybrid supercapacitors: Design, fabrication and applications. *Renewable and Sustainable Energy Reviews*, *101*, 123–145.

[25] Luan, V. H., Han, J. H., Kang, H. W., & Lee, W. (2019). Highly porous and capacitive copper oxide nanowire/graphene hybrid carbon nanostructure for high-performance supercapacitor electrodes. *Composites Part B: Engineering*, *178*, 107464.

[26] Lee, S. W., Kim, J., Chen, S., Hammond, P. T., & Shao-Horn, Y. (2010). Carbon nanotube/manganese oxide ultrathin film electrodes for electrochemical capacitors. *ACS Nano*, *4*, 3889–3896.

[27] Jiang, K. C., Xin, S., Lee, J. S., Kim, J., Xiao, X. L., & Guo, Y. G. (2012). Improved

kinetics of LiNi 1/3Mn 1/3Co 1/3O 2 cathode material through reduced graphene oxide networks. *Physical Chemistry Chemical Physics*, *14*, 2934–2939.

[28] Lee, S. H., & Im, I. H. (2018). Excellent performance hybrid supercapacitors based on LiNi1/3Mn1/3Co1/3O2/activated carbon electrode. *Materials Letters*, *231*, 38–42.

[29] Lee, S. H., & Lee, T. H. (2018). High performance hybrid supercapacitors with LiNi1/3Mn1/3Co1/3O2/activated carbon cathode and activated carbon anode. *International Journal of Hydrogen Energy*, *43*, 15365–15369.

[30] Ma, Y., Cui, P., Zhan, D., Gan, B., Ma, Y., & Liang, Y. (2019). Enhancement of the electrochemical performance of LiNi1/3Co1/3Mn1/3O2 cathode material by double-layer coating with graphene oxide and SnO2 for lithium-ion batteries. *Journal of Nanomaterials*, *2019*.

[31] Kiziltaş-Yavuz, N., Herklotz, M., Hashem, A. M., Abuzeid, H. M., Schwarz, B., Ehrenberg, H., Mauger, A., & Julien, C. M. (2013). Synthesis, structural, magnetic and electrochemical properties of LiNi 1/3Mn1/3Co1/3O2 prepared by a sol-gel method using table sugar as chelating agent. *Electrochimica Acta*, *113*, 313–321.

[32] Croy, J. R., Gutierrez, A., He, M., Yonemoto, B. T., Lee, E., & Thackeray, M. M. (2019). Development of manganese-rich cathodes as alternatives to nickel-rich chemistries. *Journal of Power Sources*, *434*, 226706.

[33] Gowda, S. R., Dees, D. W., Jansen, A. N., & Gallagher, K. G. (2015). Examining the Electrochemical Impedance at Low States of Charge in Lithium- and Manganese-Rich Layered Transition-Metal Oxide Electrodes. *Journal of The Electrochemical Society*, *162*(7), A1374–A1381.

[34] Xin, F., Zhou, H., Chen, X., Zuba, M., Chernova, N., Zhou, G., & Whittingham, M. S.

(2019). Li-Nb-O Coating/Substitution Enhances the Electrochemical Performance of the LiNi0.8Mn0.1Co0.1O2 (NMC 811) Cathode. *ACS Applied Materials and Interfaces*, *11*, 34889–34894.

[35] Mohanty, D., Sefat, A. S., Kalnaus, S., Li, J., Meisner, R. A., Andrew Payzant, E., Abraham, D. P., Wood, D. L., & Daniel, C. (2013). Investigating phase transformation in the Li1.2Co 0.1Mn0.55Ni0.15O2 lithium-ion battery cathode during high-voltage hold (4.5 V) via magnetic, X-ray diffraction and electron microscopy studies. *Journal of Materials Chemistry A*, *1*, 6249–6261.

[36] Krishna Kumar, S., Ghosh, S., & Martha, S. K. (2017). Synergistic effect of magnesium and fluorine doping on the electrochemical performance of lithium-manganese rich (LMR)-based Ni-Mn-Co-oxide (NMC) cathodes for lithium-ion batteries. *Ionics*, *23*, 1655–1662.

[37] Bettge, M., Li, Y., Gallagher, K., Zhu, Y., Wu, Q., Lu, W., Bloom, I., & Abraham, D. P. (2013). Voltage Fade of Layered Oxides: Its Measurement and Impact on Energy Density. *Journal of The Electrochemical Society*, *160*, A2046–A2055.

[38] Kumar, S. K., & Martha, S. K. (2018). Li 1.2 Mn 0.55 Ni 0.15 Co 0.1 O 2 (LMR-NMC)-Carbon Coated-LiMnPO 4 Blended Electrodes for High Performance Lithium Ion Batteries . *Journal of The Electrochemical Society*, *165*, A463–A468.

[39] Vanaphuti, P., Chen, J., Cao, J., Bigham, K., Chen, B., Yang, L., Chen, H., & Wang, Y. (2019). Enhanced Electrochemical Performance of the Lithium-Manganese-Rich Cathode for Li-Ion Batteries with Na and F CoDoping. *ACS Applied Materials and Interfaces*, *11*, 37842–37849.

[40] Jo, M. R., Kim, Y., Yang, J., Jeong, M., Song, K., Kim, Y. Il, Lim, J. M., Cho, M., Shim, J. H., Kim, Y. M., Yoon, W. S., & Kang, Y. M. (2019). Triggered reversible

phase transformation between layered and spinel structure in manganese-based layered compounds. *Nature Communications*, *10*, 1–9.

[41] Nose, M., Shiotani, S., Nakayama, H., Nobuhara, K., Nakanishi, S., & Iba, H. (2013). Na4Co2.4Mn0.3Ni0.3(PO 4)2P2O7: High potential and high capacity electrode material for sodium-ion batteries. *Electrochemistry Communications*, *34*, 266–269.

[42] Goodenough, J. B., & Kim, Y. (2010). Challenges for rechargeable Li batteries. *Chemistry of materials*, *22*, 587-603.

[43] Armand, M., & Tarascon, J. M. (2008). Building better batteries. *nature*, *451*, 652-657.

[44] Yabuuchi, N., Yoshii, K., Myung, S. T., Nakai, I., & Komaba, S. (2011). Detailed studies of a high-capacity electrode material for rechargeable batteries, Li2MnO3− LiCo1/3Ni1/3Mn1/3O2. *Journal of the American Chemical Society*, *133*, 4404-4419.

[45] Ramasamy, H. V., Kaliyappan, K., Thangavel, R., Seong, W. M., Kang, K., Chen, Z., & Lee, Y. S. (2017). Efficient method of designing stable layered cathode material for sodium ion batteries using aluminum doping. *The journal of physical chemistry letters*, *8*, 5021-5030.

[46] Di Lecce, D., Campanella, D., & Hassoun, J. (2018). Insight on the enhanced reversibility of a multimetal layered oxide for sodium-ion battery. *The Journal of Physical Chemistry C*, *122*, 23925-23933.

[47] Sagar, R. U. R., Mahmood, N., Stadler, F. J., Anwar, T., Navale, S. T., Shehzad, K., & Du, B. (2016). High capacity retention anode material for lithium ion battery. *Electrochimica Acta*, *211*, 156-163.

[48] Slater, M. D., Kim, D., Lee, E., & Johnson, C. S. (2013). Sodium-ion batteries. *Advanced Functional Materials*, *23*, 947–958.

[49] Liu, Z., Pang, G., Dong, S., Zhang, Y., Mi, C., & Zhang, X. (2019). An aqueous rechargeable sodium− magnesium mixed ion battery based on NaTi2 (PO4) 3–MnO2 system. *Electrochimica Acta, 311*, 1-7.

[50] Croy, J. R., Gutierrez, A., He, M., Yonemoto, B. T., Lee, E., & Thackeray, M. M. (2019). Development of manganese-rich cathodes as alternatives to nickel-rich chemistries. *Journal of Power Sources*, *434*, 226706.

[51] Kim, B. K., Sy, S., Yu, A., & Zhang, J. (2015). Electrochemical Supercapacitors for Energy Storage and Conversion. *Handbook of Clean Energy Systems*, 1–25.

[52] Liu, S., Wei, L., & Wang, H. (2020). Review on reliability of supercapacitors in energy storage applications. *Applied Energy*, *278*, 115436.

[53] Meet Gidwani, Anand Bhagwani, & Nikhil Rohra. (2014). Supercapacitors: the near Future of Batteries. *International Journal of Engineering Inventions (IJEI)*, *4*, 22–27.

[54] Chandra, A. (2012). Supercapacitors: An alternate technology for energy storage. *Proceedings of the National Academy of Sciences India Section A - Physical Sciences*, *82*, 79–90.

[55] Saleem, A., Desmaris, V., & Enoksson, P. (2016). Performance Enhancement of Carbon Nanomaterials for Supercapacitors. *Journal of Nanomaterials*, *2016*.

[56] Zang, X., Zhang, H., Li, C *et al.* (2014). Recent advances in porous graphene materials for supercapacitor applications. *RSC Advances, 4*, 45862-45884.

[57] Emmenegger, C., Mauron, P., Sudan, P., Wenger, P., Hermann, V., Gallay, R., & Züttel, A. (2003). Investigation of electrochemical double-layer (ECDL) capacitors electrodes based on carbon nanotubes and activated carbon materials. *Journal of Power Sources*, *124*, 321–329.

[58] Madhusanka, R., & Sitinamaluwa, H. S. (2020). *Annual Sessions of IESL 2019 Graphite-based and Graphene-based Materials for High-performance Electrochemical Capacitors : a Review*. *September, 2019*, 749-764.

[59] Tian, X., Cheng, C., Qian, L., Zheng, B., Yuan, H., Xie, S., Xiao, D., & Choi, M. M. F. (2012). Microwave-assisted non-aqueous homogenous precipitation of nanoball-like mesoporous α-Ni(OH) 2 as a precursor for NiO x and its application as a pseudocapacitor. *Journal of Materials Chemistry*, *22*, 8029–8035.

[60] Kumar, S., Saeed. G., Zhu, L *et al.* (2021). 0D to 3D carbon-based networks combined with pseudocapacitive electrode material for high energy density supercapacitor: A review. *Chemical Engineering Journal*, 403, 126352.

[61] Wu, N., Bai, X., Pan, D., Dong, B., Wei, R., Naik, N., ... & Guo, Z. (2021). Recent advances of asymmetric supercapacitors. Advanced Materials Interfaces, *8*, 2001710.

[62] Belhachemi, F., Rael, S., & Davat, B. (2000). Physical based model of power electric double-layer supercapacitors. *Conference Record - IAS Annual Meeting (IEEE Industry Applications Society)*, *5*, 3069–3076.

[63] Shukla, A. K., Ramasse, Q. M., Ophus, C., Kepaptsoglou, D. M., Hage, F. S., Gammer, C., Bowling, C., Gallegos, P. A. H., & Venkatachalam, S. (2018). Effect of composition on the structure of lithium- and manganese-rich transition metal oxides. *Energy and Environmental Science*, *11*, 830–840.

[64] Daniel, C., Mohanty, D., Li, J. *et al*.(2014). Cathode materials review. *AIP Conference Proceedings, 1597*, 26-43.

[65], Huang, W., Lin, C., Zhang, M., Li, S., Chen, Z., Zhao, W., ... & Pan, F. (2021). Revealing Roles of Co and Ni in Mn-Rich Layered Cathodes. *Advanced Energy Materials*, *11*, 2102646.

[66] Andhare, D. D., Jadhav, S. A., Khedkar, M. V., Somvanshi, S. B., More, S. D., & Jadhav, K. M. (2020). Structural and Chemical Properties of ZnFe2O4 Nanoparticles Synthesised by Chemical Co-Precipitation Technique. *Journal of Physics: Conference Series*, *1644*, 12014.

[67] Wang, X., Yang, C., Zhou, D., Wang, Z., & Jin, M. (2018). Chemical co-precipitation synthesis and properties of pure-phase BiFeO3. *Chemical Physics Letters*, *713*, 185–188.

[68] Lienstromberg, C., Pernas-Castaño, T., & Velázquez, J. J. L. (2022). Analysis of a Two-Fluid Taylor–Couette Flow with One Non-Newtonian Fluid. In *Journal of Nonlinear Science*, *32*, 24.

[69] Rudman, M. (1998). Mixing and particle dispersion in the wavy vortex regime of Taylor-Couette flow. *AIChE Journal*, *44*, 1015–1026.

[70] Van Gils, D. P. M., Bruggert, G. W., Lathrop, D. P., Sun, C., & Lohse, D. (2011). The Twente turbulent Taylor-Couette (T3C) facility: Strongly turbulent (multiphase) flow between two independently rotating cylinders. *Review of Scientific Instruments*, *82*.

[71] Ameer, G. A., Barabino, G., Sasisekharan, R., Harmon, W., Cooney, C. L., & Langer, R. (1999). Ex vivo evaluation of a Taylor-Couette flow, immobilized heparinase I device for clinical application. *Proceedings of the National Academy of Sciences of the United States of America*, *96*, 2350–2355.

[72] Schrimpf, M., Esteban, J., Warmeling, H., Färber, T., Behr, A., & Vorholt, A. J. (2021). Taylor-Couette reactor: Principles, design, and applications. *AIChE Journal*, *67*, 1–24.

[73] Hout, R., & Katz, J. (2011). Measurements of mean flow and turbulence characteristics in high-Reynolds number counter-rotating Taylor-Couette flow. *Physics of Fluids*, *23*.

[74] Altmeyer, S. (2020). Ferrofluidic Taylor Couette flow in between finite length porous cylinders with radial through-flow. *Journal of Magnetism and Magnetic Materials, 500*, 166363.

[75] Dong, S. (2007). Direct numerical simulation of turbulent Taylor - Couette flow. *Journal of Fluid Mechanics, 587*, 373–393.

[76] Uruba, V. (2018). On Reynolds number physical interpretation. *AIP Conference Proceedings*, *2000*, 20019.

[77] Rajani, B. N., Kandasamy, A., & Majumdar, S. (2009). Numerical simulation of laminar flow past a circular cylinder. *Applied Mathematical Modelling*, *33*, 1228–1247.

[78] Ismail, O. S., & Adewoye, G. T. (2012). Analyses and Modeling of Laminar Flow in Pipes Using Numerical Approach. *Journal of Software Engineering and Applications*, *05*, 653–658.

[79] Straß, A., Maier, R., & Güttel, R. (2017). Continuous Synthesis of Nanostructured Co3O4@SiO2 Core-Shell Particles in a Laminar-Flow Reactor. *Chemie-Ingenieur-Technik*, *89*, 963–967.

[80] Gutierrez, L., Gomez, L., Irusta, S., Arruebo, M., & Santamaria, J. (2011). Comparative study of the synthesis of silica nanoparticles in micromixer-microreactor and batch reactor systems. *Chemical Engineering Journal*, *171*, 674–683.

[81] Park, K. Y., Ullmann, M., Suh, Y. J., & Friedlander, S. K. (2001). Nanoparticle microreactor: Application to synthesis of titania by thermal decomposition of titanium tetraisopropoxide. *Journal of Nanoparticle Research*, *3*, 309–319.

[82] Haruna, A. B., & Ozoemena, K. I. (2019). Effects of microwave irradiation on the electrochemical performance of manganese-based cathode materials for lithium-ion

batteries. *Current Opinion in Electrochemistry*, *18*, 16–23.

[83] Kappe, C. O. (2004). Controlled microwave heating in modern organic synthesis. *Angewandte Chemie - International Edition*, *43*, 6250–6284.

[84] Clark, D. E., Folz, D. C., & West, J. K. (2000). Processing materials with microwave energy. *Materials Science and Engineering A*, *287*, 153–158.

[85] Nkosi, F., Palaniyandy, N., Raju, K., & Ozoemena, K. I. (2020). Influence of Microwave Irradiation and Combustion Fuels on the Rate Capability and Cycle Performance of Li1.2Mn0.52Ni0.13Co0.13Al0.02O2 Layered Material. *Electroanalysis*, *32*, 3159–3169.

[86] Li, L., Chang, Y. L., Xia, H., Song, B. H., Yang, J. R., Lee, K. S., & Lu, L. (2014). NH4F surface modification of Li-rich layered cathode materials. *Solid State Ionics*, *264*, 36–44.

[87] Gür, T. M. (2018). Review of electrical energy storage technologies, materials and systems: Challenges and prospects for large-scale grid storage. *Energy and Environmental Science*, *11*, 2696–2767.

[88] Lee, J. H., Kim, H. K., Baek, E., Pecht, M., Lee, S. H., & Lee, Y. H. (2016). Improved performance of cylindrical hybrid supercapacitor using activated carbon/ niobium doped hydrogen titanate. *Journal of Power Sources*, *301*, 348–354.

[89] Xu, N., Sun, X., Zhao, F., Jin, X., Zhang, X., Wang, K., Huang, K., & Ma, Y. (2017). The Role of Pre-Lithiation in Activated Carbon/Li4Ti5O12 Asymmetric Capacitors. *Electrochimica Acta*, *236*, 443–450.

[90] Naoi, K. (2010). "Nanohybrid capacitor": The next generation electrochemical capacitors. *Fuel Cells*, *10*, 825–833.

[91] Naoi, K., Ishimoto, S., Miyamoto, J. I., & Naoi, W. (2012). Second generation

"nanohybrid supercapacitor": Evolution of capacitive energy storage devices. *Energy and Environmental Science*, *5*, 9363–9373.

[92] Zheng, J., Deng, S., Shi, Z., Xu, H., Xu, H., Deng, Y., Zhang, Z., & Chen, G. (2013). The effects of persulfate treatment on the electrochemical properties of Li[Li 0.2Mn 0.54Ni 0.13Co 0.13]O 2 cathode material. *Journal of Power Sources*, *221*, 108–113.

[93] Thapa, A. K., Lavery, B. W., Hona, R. K., Sapkota, N., Koralalage, M. K., Adeniran, A., Ajayi, B. P., Zain, M. A., Wang, H., Druffel, T., Jasinski, J. B., Sumanasekera, G. U., Sunkara, M. K., & Yoshio, M. (2022). Mn-Rich NMC Cathode for Lithium-Ion Batteries at High-Voltage Operation, *Energies*, *15*, 8357.

[94] Nkosi, F. P., Palaniyandy, N., Raju, K., Billing, C., & Ozoemena, K. I. (2019). Physico-chemistry of energy-dense Li1.2Mn0.52Co0.13Ni0.13Al0.02O2 cathode material for lithium-ion batteries obtained from urea and ethylene glycol fuels. *Materials Research Express*, *6*, 115501.

[95] Mohanty, D., Sefat, A. S., Li, J., Meisner, R. A., Rondinone, A. J., Payzant, E. A., Abraham, D. P., Wood, D. L., & Daniel, C. (2013). Correlating cation ordering and voltage fade in a lithium-manganese-rich lithium-ion battery cathode oxide: A joint magnetic susceptibility and TEM study. *Physical Chemistry Chemical Physics*, *15*, 19496–19509.

[96] Lukatskaya, M. R., Dunn, B., & Gogotsi, Y. (2016). Multidimensional materials and device architectures for future hybrid energy storage. *Nature Communications*, *7*, 12647.

[97] Chen, G. Z. (2021). Linear and non-linear pseudocapacitances with or without diffusion control. *Progress in Natural Science: Materials International*, *31*, 792–800.

[98] Fu, G., Li, H., Bai, Q., Li, C., Shen, Y., & Uyama, H. (2021). Dual-doping activated

carbon with hierarchical pore structure derived from polymeric porous monolith for high performance EDLC. *Electrochimica Acta*, *375*, 137927.

[99] Ozoemena, K. I., Raju, K., Ejikeme, P. M., & Ozoemena, K. I. (2017). High-performance Mn3O4/onion-like carbon (OLC) nanohybrid pseudocapacitor: Unravelling the intrinsic properties of OLC against other carbon supports. *Carbon*, *117*, 20–32.

[100] Mofokeng, T. P., Tetana, Z. N., & Ozoemena, K. I. (2020). Defective 3D nitrogen-doped carbon nanotube-carbon fibre networks for high-performance supercapacitor: Transformative role of nitrogen-doping from surface-confined to diffusive kinetics. *Carbon*, *169*, 312–326.

[101] Mei, B. A., Lau, J., Lin, T., Tolbert, S. H., Dunn, B. S., & Pilon, L. (2018). Physical Interpretations of Electrochemical Impedance Spectroscopy of Redox Active Electrodes for Electrical Energy Storage. *Journal of Physical Chemistry C*, *122*, 24499–24511.

[102] Bo, Z., Wen, Z., Kim, H., Lu, G., Yu, K., & Chen, J. (2012). One-step fabrication and capacitive behavior of electrochemical double layer capacitor electrodes using vertically-oriented graphene directly grown on metal. *Carbon*, *50*, 4379–4387.

[103] Wang, H. W., Hu, Z. A., Chang, Y. Q., Chen, Y. L., Zhang, Z. Y., Yang, Y. Y., & Wu, H. Y. (2011). Preparation of reduced graphene oxide/cobalt oxide composites and their enhanced capacitive behaviors by homogeneous incorporation of reduced graphene oxide sheets in cobalt oxide matrix. *Materials Chemistry and Physics*, *130*, 672–679.

[104] Taberna, P. L., Simon, P., & Fauvarque, J. F. (2003). Electrochemical Characteristics and Impedance Spectroscopy Studies of Carbon-Carbon Supercapacitors. *Journal of The Electrochemical Society*, *150*, A292-A300.

[105] Ganesh, V., Pitchumani, S., & Lakshminarayanan, V. (2006). New symmetric and

asymmetric supercapacitors based on high surface area porous nickel and activated carbon. *Journal of Power Sources*, *158*, 1523–1532.

[106] Macdonald, J.R. (1987). Interpretation of electrochemical Impedance Spectroscopy. The electrical Equivalent Circuit. *Journal of Electrochemical Society*, *134*, 1679-1686.

[107] Kumar, R., Shukla, P. S., Varma, G. D., & Bag, M. (2021). Synthesis of porous electrode from CH3NH3PbBr3 single crystal for efficient supercapacitor application: Role of morphology on the charge storage and stability. *Electrochimica Acta*, *398*, 139344.

[108] Shaheen, A., Hussain, S., Qiao, G. J., Mahmoud, M. H., Fouad, H., & Akhtar, M. S. (2022). Nanosheets Assembled Co 3 O 4 Nanoflowers for Supercapacitor Applications . *Journal of Nanoelectronics and Optoelectronics*, *16*, 1357–1362.

[109] Zhang, B. H., Liu, Y., Chang, Z., Yang, Y. Q., Wen, Z. B., & Wu, Y. P. (2014). Nanowire K0.19MnO2 from hydrothermal method as cathode material for aqueous supercapacitors of high energy density. *Electrochimica Acta*, *130*, 693–698.

[110] Zhao, Z., Ye, Y., Zhu, W., Xiao, L., Deng, B., & Liu, J. (2018). Bismuth oxide nanoflake@carbon film: A free-standing battery-type electrode for aqueous sodium ion hybrid supercapacitors. *Chinese Chemical Letters*, *29*, 629–632.

[111] Li, J., Liu, Z., Zhang, Q., Cheng, Y., Zhao, B., Dai, S., Wu, H. H., Zhang, K., Ding, D., Wu, Y., Liu, M., & Wang, M. S. (2019). Anion and cation substitution in transition-metal oxides nanosheets for high-performance hybrid supercapacitors. *Nano Energy*, *57*, 22–33.

[112] Priyadharsini, N., & Selvan, R. K. (2017). Nano-sheet-like KNiPO4 as a positive electrode material for aqueous hybrid supercapacitors. *Electrochimica Acta*, *246*, 963–970.

[113] Luan, Y., Zhang, H., Yang, F., Yan, J., Zhu, K., Ye, K., Wang, G., Cheng, K., & Cao, D. (2018). Rational design of NiCo 2 S 4 nanoparticles @ N-doped CNT for hybrid supercapacitor. *Applied Surface Science*, *447*, 165–172.

[114] Zhou, C., Zhang, Y., Li, Y., & Liu, J. (2013). Construction of high-capacitance 3D CoO@ polypyrrole nanowire array electrode for aqueous asymmetric supercapacitor. *Nano letters*, *13*, 2078-2085.

[115] Li, R., Lin, Z., Ba, X., Li, Y., Ding, R., & Liu, J. (2016). Integrated copper-nickel oxide mesoporous nanowire arrays for high energy density aqueous asymmetric supercapacitors. *Nanoscale Horizons*, *1*, 150–155.